View metadata, citation and similar papers at core.ac.uk

brought to you by CORE

provided by Online Research Database In Technology

Technical University of Denmark

What ignites on the neutron star of 4U0614+091?

Kuulkers, E.; in 't Zand, J.J.M.; Atteia, J.-L.; Levine, A.M.; Brandt, Søren; Smith, D.A.; Linares, M.; Falanga, M.; Sanchez-Fernandez, C.; Markwardt, C.B.; Strohmayer, T.E.; Cumming, A.; Suzuki, M.

Published in:
Astronomy & Astrophysics

Link to article, DOI:
10.1051/0004-6361/200913210

Publication date:
2010

Document Version
Publisher's PDF, also known as Version of record

Link back to DTU Orbit

Citation (APA):
Kuulkers, E., in 't Zand, J. J. M., Atteia, J-L., Levine, A. M., Brandt, S. K., Smith, D. A., ... Suzuki, M. (2010). What ignites on the neutron star of 4U0614+091? Astronomy & Astrophysics, 514(9). DOI: 10.1051/0004-6361/200913210

DTU Library
Technical Information Center of Denmark

General rights
Copyright and moral rights for the publications made accessible in the public portal are retained by the authors and/or other copyright owners and it is a condition of accessing publications that users recognise and abide by the legal requirements associated with these rights.

- Users may download and print one copy of any publication from the public portal for the purpose of private study or research.
- You may not further distribute the material or use it for any profit-making activity or commercial gain
- You may freely distribute the URL identifying the publication in the public portal

If you believe that this document breaches copyright please contact us providing details, and we will remove access to the work immediately and investigate your claim.

A&A 514, A65 (2010)
DOI: 10.1051/0004-6361/200913210
© ESO 2010

Astronomy & Astrophysics

What ignites on the neutron star of 4U 0614+091?

E. Kuulkers[1], J. J. M. in 't Zand[2], J.-L. Atteia[3], A. M. Levine[4], S. Brandt[5], D. A. Smith[6], M. Linares[7], M. Falanga[8], C. Sánchez-Fernández[1], C. B. Markwardt[9], T. E. Strohmayer[10], A. Cumming[11], and M. Suzuki[12]

[1] ISOC, ESA, European Space Astronomy Centre (ESAC), PO Box 78, 28691 Villanueva de la Cañada (Madrid), Spain
e-mail: Erik.Kuulkers@esa.int
[2] SRON Netherlands Institute for Space Research, Sorbonnelaan 2, 3584 CA Utrecht, The Netherlands
[3] Laboratoire d'Astrophysique de Toulouse-Tarbes, Observatoire Midi-Pyrénées (CNRS-UMR5572/Université Paul Sabatier Toulouse III), 14 avenue Édouard Belin, 31400 Toulouse, France
[4] Kavli Institute for Astrophysics and Space Research, Massachusetts Institute of Technology, Cambridge, MA 02139, USA
[5] National Space Institute, DTU, Juliane Maries Vej 30, 2100 Copenhagen, Denmark
[6] Guilford College, Physics Department, 5800 West Friendly Ave., Greensboro, NC 27410, USA
[7] Astronomical Institute "Anton Pannekoek", University of Amsterdam and Center for High-Energy Astrophysics, PO Box 94249, 1090 GE, Amsterdam, The Netherlands
[8] International Space Science Institute, Hallerstrasse 6, 3012 Bern, Switzerland
[9] UMD/CRESST/GSFC, Greenbelt, MD 20771, USA
[10] Astrophysics Science Division, NASA/GSFC, Greenbelt, MD 20771, USA
[11] Physics Department, McGill University, 3600 rue University, Montreal, QC, H3A 2T8, Canada
[12] ISS Science Project Office ISAS, JAXA, 2-1-1 Sengen, Tsukuba, Ibaraki 305-8505, Japan

Received 31 August 2009 / Accepted 4 February 2010

ABSTRACT

The low-mass X-ray binary 4U 0614+091 is a source of sporadic thermonuclear (type I) X-ray bursts. We find bursts with a wide variety of characteristics in serendipitous wide-field X-ray observations by the WATCH on *EURECA*, the ASM on *RXTE*, the WFCs on *BeppoSAX*, the FREGATE on *HETE-2*, the IBIS/ISGRI on *INTEGRAL*, and the BAT on *Swift*, as well as pointed observations with the PCA and HEXTE on *RXTE*. Most of the bursts are bright, i.e., they reach a peak flux of about 15 Crab, but a few are weak and only reach a peak flux below a Crab. One of the bursts shows a very strong photospheric radius-expansion phase. This allows us to evaluate the distance to the source, which we estimate to be 3.2 kpc. The burst durations vary generally from about 10 s to 5 min. However, after one of the intermediate-duration bursts, a faint tail is seen to at least about 2.4 h after the start of the burst. One very long burst was observed, which lasted for several hours. This superburst candidate was followed by a normal type-I burst only 19 days later. This is, to our knowledge, the shortest burst-quench time among the superbursters. The observation of a superburst in this system is difficult to reconcile if the system is accreting at about 1% of the Eddington limit. We describe the burst properties in relation to the persistent emission. No strong correlations are apparent, except that the intermediate-duration bursts occurred when 4U 0614+091's persistent emission was lowest and calm, and when bursts were infrequent (on average roughly one every month to 3 months). The average burst rate increased significantly after this period. The maximum average burst recurrence rate is about once every week to 2 weeks. The burst behaviour may be partly understood if there is at least an appreciable amount of helium present in the accreted material from the donor star. If the system is an ultra-compact X-ray binary with a CO white-dwarf donor, as has been suggested, this is unexpected. If the bursts are powered by helium, we find that the energy production per accumulated mass is about 2.5 times less than expected for pure helium matter.

Key words. accretion, accretion disks – binaries: close – stars: individual: 4U 0614+091 – stars: neutron – X-rays: binaries – X-rays: bursts

1. Introduction

Type I X-ray bursts (Grindlay et al. 1975; Belian et al. 1976; Hoffman et al. 1978, hereafter bursts) result from thermonuclear shell flashes on a neutron star, which is caused by the ignition of either He and/or H-rich material supplied by a binary companion star (Hansen & van Horn 1975; Woosley & Taam 1976; Maraschi & Cavaliere 1977; Lamb & Lamb 1978; for reviews see Lewin et al. 1993; Strohmayer & Bildsten 2006). Bursts generally appear as short transient events wherein the X-ray intensity rises rapidly on a time scale of seconds, and decays in an exponential fashion back to the pre-burst level. The decay lasts almost always longer than the rise. Burst durations range from several seconds up to half an hour. The burst spectra generally harden during the rise and soften during the decay. This has been attributed to the heating and cooling of the uppermost layers of the neutron star. The spectra can be satisfactorily described by black-body emission from spherical regions with radii of around 10 km at inferred temperatures up to $kT \simeq 3$ keV. The burst-to-burst time intervals are typically of the order of hours to days. They are thought to be determined by the time for the neutron star to accumulate enough fuel to power another burst.

Under certain conditions, the local luminosity may reach or exceed the Eddington limit and matter may be pushed outward. As a result, the neutron star photosphere also moves outward. Consequently, the emitting area increases and the observed inferred black-body temperature drops. When the surge of energy release is over, the photosphere gradually returns to its pre-burst

radius. During this phase, the emitting area decreases and the inferred temperature increases. During the expansion and contraction phase, the luminosity is expected to be close to the Eddington limit. After the photosphere recedes to its pre-burst radius (called "touch-down") cooling is typically observed. Such bursts are referred to as photospheric radius-expansion type I X-ray bursts (e.g., Lewin et al. 1984; Tawara et al. 1984, hereafter radius-expansion bursts).

A few bursts last hours to half a day (Cornelisse et al. 2000; Strohmayer & Brown 2002; for a review see, e.g., Kuulkers 2004). Such bursts show the same characteristics as the typical bursts described above, except that the energy output is about a thousand times higher. They recur on time scales of months to years. Their origin is different from the typical bursts, because they are thought to be due to unstable burning of C deeper in the neutron star envelope (Cumming & Bildsten 2001; Strohmayer & Brown 2002). These long events are called superbursts (Wijnands 2001). Typical bursts are seen up to the time of the superbursts. However, they cease to occur after the superburst, for up to about a month (see, e.g., Cornelisse et al. 2002a; Kuulkers et al. 2002a). This is thought to be due to the superburst heating up the surface layer, and therefore preventing the unstable ignition of H and/or He (Cumming & Macbeth 2004).

There are also bursts that have durations and energy releases intermediate between typical bursts and superbursts. They are referred to as intermediate-duration X-ray bursts (Cumming et al. 2006; hereafter intermediate-duration bursts). They show decay times ranging from several to tens of minutes and energy outputs of about 10^{41} erg. Most of these events occur in sources with low persistent luminosity ($L_{\rm pers} \lesssim 0.01\ L_{\rm Edd}$, where $L_{\rm Edd}$ represents the Eddington luminosity) and are thought to be due to flashes of relatively thick He layers in ultra-compact X-ray binaries (UCXBs; i.e., low-mass X-ray binaries with an orbital period less than an hour), see in 't Zand et al. (2005), Cumming et al. (2006), Falanga et al. (2008), and references therein. The intermediate-duration bursts in the H-rich and luminous system GX 17+2 (Kuulkers et al. 2002b) probably have a different origin.

The low-mass X-ray binary 4U 0614+091 has long been known to be a source of bursts, but this identification was based on the detections of only several of them, with relatively poor, ~1°, position determinations[1], as well as coarse timing and/or X-ray spectral information (Lewin 1976; Swank et al. 1978; Brandt et al. 1992, 1993a,b; Brandt 1994; Brandt & Lund 1995). More recently, an hours-long flare was reported, which showed characteristics resembling superbursts (Kuulkers 2005; see Sect. 3.2). Brandt et al. (1992) used the observation with *GRANAT*/WATCH of a peak burst flux of ~10 Crab (6−20 keV) to infer, assuming this peak flux does not exceed the Eddington limit for a 1.4 $M_\odot$ neutron star with a He-rich atmosphere, that the source distance must be about 3.2 kpc. 4U 0614+091 is, therefore, one of the closest to Earth of the known actively bursting systems (see, e.g., Jonker & Nelemans 2004; Galloway et al. 2008).

In the last decade, *HETE-2* triggered thirteen times on bursts from 4U 0614+091. Moreover, three strong bursts from 4U 0614+091 triggered the γ-ray burst monitors on board *INTEGRAL* (see Chelovekov et al. 2007) and *Swift*. Strohmayer et al. (2008) discovered burst oscillations near 415 Hz in one of the brightest *Swift*/BAT bursts.

[1] Note that spatially the closest known X-ray burster to 4U 0614+091 is MXB 0513−40, with a distance of 51°.

It is difficult to understand 4U 0614+091 as the origin of bursts. Since it is thought to be an UCXB (in 't Zand et al. 2007; Shahbaz et al. 2008, and references therein), it is supposed to be so compact that the donor star can only be a non-degenerate H-deficient star or a white dwarf. Evolutionary models suggest that the accreted material could be rich in C/O or He (Nelemans et al. 2010). However, no evidence of He (or H) has been found so far in optical spectra, with rather stringent upper limits: He and/or H are at most present at the 10% level (Werner et al. 2006). These spectra suggest the donor star to be a C/O white dwarf (Nelemans et al. 2003, 2006; Werner et al. 2006). This seems to be at odds (see Juett et al. 2001; Juett & Chakrabarty 2003) with the fact that we see bursts in 4U 0614+091, which are usually understood as being due to unstable ignition of He or H. Moreover, 4U 0614+091 is an interesting case among the sources showing superbursts. Superbursts are expected to occur only in systems with accretion rates in excess of about 10% of the Eddington rate, i.e., the rate which yields emission at the Eddington limit (Cumming & Bildsten 2001; Strohmayer & Brown 2002). However, the low persistent X-ray luminosity of 4U 0614+091 indicates an accretion rate which is an order of magnitude lower (e.g., Ford et al. 2000).

In this paper we report on the detection of bursts from 4U 0614+091 made with various instruments. In Sects. 2.1 and 2.2 we describe the instruments and the data analyses of the bursts seen between 1992 and 2007, as well as the analysis of the persistent emission. We complement this with information extracted for the bursts seen before 1992 (Sect. 2.3). An overview of all the typical and intermediate-duration bursts seen appears in Sect. 3.1. We collectively refer to both types of bursts as normal bursts. One of them is a radius-expansion burst; it is discussed in Sect. 3.1.2. We then describe the results of our analysis of the superburst (Sect. 3.2), our burst oscillation search (Sect. 3.3), and the characteristics of the persistent emission of the source (Sect. 3.4). Finally, we show the long-term X-ray behaviour of 4U 0614+091 (Sect. 3.5) and close the paper with a discussion of our results (Sect. 4).

2. Observations and data analysis

Almost all the observations between 1992 and 2007 described in this paper were serendipitously obtained using six different X-ray instruments on just as many space-borne observatories, see Table 1. Only the observations with the *RXTE*/PCA and *RXTE*/HEXTE were purposely dedicated to 4U 0614+091. In the next subsections we describe these instruments and the analysis of the data in more detail. We usually refer to the instruments by acronyms only. In Table 1 we also give the total time of exposure for observations with 4U 0614+091 in the field of view and the total number of bursts detected from this source in these observations.

2.1. Observations and instrument-specific data analysis issues

2.1.1. *EURECA* WATCH

EURECA (EUropean REtrievable CArrier) carried the Wide Angle Telescope for Cosmic Hard X-rays (WATCH; Lund 1985; Brandt et al. 1990). WATCH operated from August 1992 to June 1993. It comprised a rotating modulation collimator (RMC) and yielded images through a cross-correlation method. It viewed a circular field with a radius of about 65°, was sensitive between 6 and 150 keV, and had an effective area of

Table 1. Overview of instruments that have detected bursts from 4U 0614+091 between 1992 and 2007.

Time span	Satellite/Instrument	$E_{\rm sens}$[a] (keV)	$t_{\rm exp}$[b] (days)	n[c]
Aug. 1992–Jun. 1993	*EURECA*/WATCH	6–150	∼50	3
Dec. 1995–Aug. 2007	*RXTE*/ASM	1.5–12	≃58	7
Dec. 1995–Aug. 2007	*RXTE*/PCA	2–60	≃23	2
Dec. 1995–Aug. 2007	*RXTE*/HEXTE	15–250	≃23	2
Apr. 1996–Apr. 2002	*BeppoSAX*/WFC	2–28	≃27	1
Oct. 2000–Mar. 2007	*HETE-2*/FREGATE	6–400	∼194	13
Oct. 2002–Aug. 2007	*INTEGRAL*/ISGRI	15–1000	≃22	2
Oct. 2002–Aug. 2007	*INTEGRAL*/JEM-X	3–35	≃0.8	0
Nov. 2004–Aug. 2007	*Swift*/BAT	15–150	≃26[d]	2

Notes. [(a)] Nominal sensitive energy range; [(b)] total observation net exposure time; [(c)] number of bursts seen; [(d)] total effective exposure time (corrected for off-axis response).

about 45 cm^2. For events with a duration longer than the rotation period of the RMC (≃1 s), the relative position accuracy was better than 1°, and, in favourable cases, was as good as about 0.1°. The flux sensitivity was about 100 mCrab in one day.

4U 0614+091 was located in the ≃1 steradian field of view from mid January 1993 until the end of April 1993, with an observing efficiency of a little more than 40%. *EURECA*/WATCH observed a total of three bursts during that time. Preliminary reports of these events can be found in Brandt et al. (1993a,b), Brandt (1994) and Brandt & Lund (1995).

For our analysis, we used count rates as a function of time along with vignetting estimates for the source. Background rates were determined by polynomial fits to the count rates outside the intervals of each burst. We define the 3σ confidence level above which we regard a signal as significant as 3 times the square root of the number of background counts in each time bin.

2.1.2. *RXTE* All-Sky Monitor

2.1.2.1 Scanning Shadow Cameras. The Rossi X-ray Timing Explorer (*RXTE*; launched December 1995) All-Sky Monitor (ASM) consists of three Scanning Shadow Cameras (SSCs, hereafter called SSC0, SSC1 and SSC2; Levine et al. 1996). Each SSC views a 12° × 110° (full-width at zero response, *FWZR*) field through a random-slit coded mask. The field of view of one SSC is 90° from the colocated field centres of the other two SSCs. The assembly holding the three SSCs is generally held stationary for a 90 s "dwell". A drive then rotates this assembly through 6° between dwells. This yields good sky coverage: as much as 80% of the X-ray sky is covered every 90 min orbit around the Earth.

For each dwell, histograms of counts ("raw" counts, i.e., not corrected for transmission, sources in the field of view, background, etc.) as a function of position in each detector are recorded for three energy bands (roughly 1.5−3, 3−5, 5−12 keV). Also, the total number of counts registered in each SSC are recorded in 1/8 s time-series bins in the same energy bands. For observations done before March 2001 (MJD 51 970), there is imaging data integrated over entire dwells, and count rate data with no imaging information. Since March 2001 event-by-event data are telemetered so that both temporal and imaging information can be extracted for portions of dwells. For sources away from bright sources, the sensitivity is roughly 10−15 mCrab (1σ in the 1.5−12 keV band) for a reliable single-dwell source detection; multi-day averaging improves the sensitivity down to about a few mCrab. The average intensity of each known source in the field of view is determined by the instrument team through an analysis of the coded-aperture data and is made available via the internet, on a dwell by dwell basis as well as 1-day averages[2].

The intensity history of 4U 0614+091 up to September 2007 was obtained from each of 62 720 dwells, more or less evenly spread over the years (see also Sect. 3.5.1). We used the following method to search for bursts: 1) identify candidate dwells in which the source intensity minus its uncertainty was larger than the overall mean intensity of 4U 0614+091 by 4 times the rms uncertainty in the overall mean intensity; 2) visually inspect raw count rates at 1-s time resolution within the candidate dwells for evidence of burst-like temporal behaviour; 3) use the hardness ratios, defined as the time-bin-wise ratios of the count rates in the 5−12 keV band to those in the 1.5−5 keV band, to verify the typical hard-to-soft behaviour of bursts. Note that this technique is not suitable for bursts that last substantially longer than a dwell or for bursts that do not start within a dwell. Our search yielded 6 bursts and one superburst.

2.1.2.2 (Time-resolved) X-ray spectral analysis of ASM data. The 3-channel ASM data can constrain simple spectral models like power laws and black-body radiation (see, e.g., Ford et al. 1996; Kuulkers 2002; Keek et al. 2008). In our spectral analyses we employed the same method as in Keek et al. (2008). This includes calibrations of the source flux with average ASM data of the Crab over 200-day intervals around each data point.

The spectral analysis can also be satisfactorily applied to raw ASM data when dealing with bursts. If one assumes that the burst emission is not influenced by persistent emission (see, e.g., Kuulkers et al. 2002b), net-burst count rates can be obtained by subtracting the average raw pre-burst count rates from the raw burst count rates. If one also knows the celestial position of the burst, the effective mask/collimator transmission can be computed. This allows the estimation of equivalent on-axis net burst count rates for the given energy bands and these, after renormalization with the Crab as described above, can be fit with a black-body spectrum model. Whenever a burst was simultaneously observed by two SSCs we combined the renormalized net count rate information from the two cameras. We derived the three-channel transmission-corrected net-burst spectra from the 1-s raw count rates. We calculated the errors by taking square roots of the numbers of counts per each time bin. We started with a spectral time bin size of 1 s (2S 0918−549, see below) or 2 s (4U 0614+091). Each time the net-burst rates following the peak decreased by a factor of $\sqrt{2}$, we doubled the spectral time-bin size.

Since all the corrections may introduce errors in our analysis of the raw ASM data, we first applied our method to bursts from 2S 0918−549 that, like 4U 0614+091, lies in a relatively empty field in the sky (spatially the closest bursters to 2S 0918−549 are EXO 0748−676 at ≃16° away and the transient GS 0836−429 at ≃14° away). 2S 0918−549 is similar to 4U 0614+091 in that it is also thought to be an UCXB which shows low persistent accretion and infrequent bursts (see, e.g., in 't Zand et al. 2005). Most of the 2S 0918−549 bursts show a radius-expansion phase. By comparing the ASM time-resolved X-ray burst spectral analysis to that derived from high-quality X-ray spectra observed

[2] http://heasarc.gsfc.nasa.gov/docs/xte/asm_products.html and http://xte.mit.edu/ASM_lc.html

with well-calibrated detectors, one can verify our ASM burst-spectral analysis method.

We searched the ASM data on 2S 0918−549 for bursts using the same algorithm as that used for 4U 0614+091. We found 5 bursts (see Table A.1) over the more than ≃11 year time span of observations, with a net effective exposure time of 47.8 days between 1996 January and 2007 August. Three of them were already noted by in 't Zand et al. (2005); our third X-ray burst, which occurred on UT 2002 August 23, was not noted by them probably due of its weakness (because of relatively low transmission, see Table A.1). By comparing our ASM time-resolved spectral fit results with those for the bursts seen with the WFC (see in 't Zand et al. 2005) and PCA (see Galloway et al. 2008), we find comparable values for all spectral parameters. The ASM spectral fits show similar kind of radius expansion phases which reach similar derived peak fluxes as the other instruments. We, therefore, conclude that our time resolved X-ray spectral analysis of the raw ASM data gives consistent results with that seen from other instruments, and therefore our method can be trusted.

2.1.3. *RXTE* PCA and HEXTE

The Proportional Counter Array (PCA; Bradt et al. 1993; Jahoda et al. 2006) onboard *RXTE* provides a large collecting area (maximum net geometric area of about 8000 cm^2) and high time resolution (down to μs). It consists of 5 proportional counter units (PCUs) behind 1° (full-width at half maximum, *FWHM*) collimators. It is sensitive in the 2−60 keV range down to ≃0.2 mCrab.

The High-Energy X-ray Timing Experiment (15−250 keV; Rothschild et al. 1998) onboard the same satellite consists of 8 detectors with a total area of about 1600 cm^2. The 8 detectors are split up in two clusters of 4 each. During normal operations, each cluster is alternately pointed on and off the source generally every 16 or 32 s, to provide near real-time background measurements (note that at the end of 2006 cluster A was fixed to always view the source). HEXTE can measure a typical X-ray source down (at the 3σ level) to about 1 mCrab up to ≃100 keV in 10^5 s.

We first inspected the light curves at 1 s time resolution of all the publicly available PCA data up to September 2007 on 4U 0614+091 that was collected in the Standard 1 mode. A couple of strong burst-like events were seen; all except one were due to detector-related events. The one celestial event occurred simultaneously with the burst seen by FREGATE, on UT 2001 February 4 (MJD 51 944; see Sect. 2.1.5). Only the first 30 s of the event were covered, after which the PCA was shut off because the count rate (>55 kct s^{-1}) exceeded the "High Rate Monitor" safety threshold. Apart from the first 30 s of the burst, the PCA also observed the tail of the burst. In observations taken on UT 2000 September 2 (MJD 51 789) we found the tail of another burst for which the onset was missed.

We used version 6.5 of the HEASOFT software suite for our *RXTE* data analysis. For the time-resolved analysis of the prompt burst on MJD 51 944 we used the PCA data from either Event mode or Burst Catcher mode when available (the high count rates reached during the maximum of the burst resulted in data losses near the ends of the 1 s buffers of the Event mode). These modes provided numbers of counts in 64 channels covering the PCA energy range at time resolutions of 122 μs and 8 ms, respectively. At the time the prompt burst occurred, 4 PCUs (PCU 0−3) were on; the data from all layers and all PCUs were automatically combined in these modes. During the spike (see Sect. 3.1.2) we created time-resolved spectra at 2 ms resolution. During the rest of the prompt burst, we used a time resolution of 0.125 s. Although the majority of the prompt burst was observed by HEXTE, we do not use the HEXTE data for the burst spectral analysis because data from a broader energy range (7−400 keV) was obtained by FREGATE (see Sect. 2.1.5). For the tail of the bursts on MJD 51 789 and MJD 51 944 we used the PCA data from the Standard 2 mode; this mode provides counts in 129 channels covering the PCA energy range with a time resolution of 16 s. We formed spectra averaged over 112 s intervals from the events occurring in all layers of the PCUs which were on during and before or after the burst; this was PCU 3 on MJD 51 944 and PCUs 2, 3 on MJD 51 789.

Dead-time correction is only possible for all spectra with a time resolution equal or higher than 0.125 s. We subtracted the pre-burst persistent emission from the burst emission. Our time-resolved burst spectral fits of PCA data covered the 3 to 20 keV energy band. We included a 1% systematic uncertainty in each spectral bin in addition to the usual statistical uncertainties.

We extracted information on the persistent emission only when *RXTE* data was available within 1 day of a burst (see Sect. 3.4). We did this for data from both the PCA and HEXTE by applying standard criteria, i.e., by filtering out data taken at elevations less than 10° or with an offset from the source greater than 0.02°. Also, we created instrument response and background files following the standard analysis threads using the latest information available[3]. We corrected the count-rate spectra for dead-time losses. For the PCA we only used PCU 2 data (across the *RXTE* mission this PCU has the highest duty cycle) obtained with the Standard 2 mode. Pulse-height spectra were formed from the events from all layers and we included a 1% systematic uncertainty in each spectral bin. We performed fits to the persistent emission in the 3−30 keV and 17−100 keV bands for the PCA and HEXTE, respectively. A multiplicative constant was applied to the HEXTE spectra to account for the uncertainty in the relative normalizations of the instruments, i.e., both HEXTE Cluster A and B were allowed to vary with respect to the PCA. This multiplicative factor was found to be between 0.6 and 0.8.

For the comparison (see Sect. 3.1.2) of the burst observed on MJD 51 944 with that of the superbursts of 4U 1820−303 (Strohmayer & Brown 2002) and 4U 1636−536 (Strohmayer & Markwardt 2002) at hard X-ray energies, we extracted light curves from data obtained by HEXTE in the 15−60 keV band. In this process we applied the same standard filtering criteria as those described above. We corrected the light curves for dead time and background following the standard procedures[4], and normalized them to the Crab count rate in the same energy band. For this analysis we only used the Standard Modes (Archive Spectral Bin, 64-bin spectra produced every 16 s) data from Cluster A.

To characterise the overall spectral behaviour of 4U 0614+091 we created so-called colour−colour and hardness-intensity diagrams (CD and HID, respectively). All publicly available pointed PCA observations of 4U 0614+091 up to September 2007 were used. We extracted background and dead-time corrected count rates from the Standard 2 data using the same standard procedures and filtering criteria as applied to the spectral data, with 16 s time resolution. We used the following energy bands: 2.0−3.5 keV (A),

[3] http://heasarc.nasa.gov/docs/xte/data_analysis.html
[4] http://heasarc.gsfc.nasa.gov/docs/xte/recipes/hexte.html

3.5−6.0 keV (B), 6.0−9.7 keV (C), and 9.7−16.0 keV (D). We define the soft and hard colours (SC, HC) as the ratios of the count rates in the various bands: SC = B/A and HC = D/C; the intensity (Int) is defined as the sum of the count rates in the four energy bands: Int = A + B + C + D. We normalized both the colours and intensity to the Crab values nearest in time to account for changes in detector gas gain (see, e.g., Kuulkers et al. 1994; van Straaten et al. 2003). Since the values do not change significantly within an observation (i.e., on time scales of order an hour), they were averaged over one observation.

2.1.4. *BeppoSAX* Wide-Field Cameras

The Wide-Field Cameras (WFCs; Jager et al. 1997) were two identical coded-aperture instruments onboard the *BeppoSAX* satellite (Satellite per Astronomia X; Boella et al. 1997), which were operated between April 1996 and April 2002. The field of view was 40° × 40° (*FWZR*), the angular resolution 5′ (*FWHM*) and the source-location accuracy was generally better than 1′ (99% confidence). The detectors were sensitive to the energy range 2 to 28 keV and had a net collecting area of 140 cm^2. The on-axis detection threshold was of the order of 0.3 Crab for a 1 s observation and a few mCrab for a 10^5 s observation.

The WFCs pointed in opposite directions with respect to each other and perpendicular to the Narrow-Field Instruments (NFIs) on the same satellite. Since the pointing directions of the WFCs were usually governed by the observations of the NFIs, the WFC sky coverage was not uniform. 4U 0614+091 was mostly seen at large off-axis angles.

We extracted the reconstructed source flux in the 2−25 keV bandpass with a time resolution of 2 s whenever 4U 0614+091 was in the field of view. We also extracted information on all photons detected on the appropriate detector with varying time resolutions between 0.5 and 8 s. Light curves were formed from both the fluxes and the photon rate data. Bursts were searched for by eye as well using an automatic algorithm (see Cornelisse et al. 2003). We found only one burst.

For the generation of WFC X-ray spectra we first cross-correlated the detector data with the expected imaging response of WFC unit 2 for 4U 0614+091 (see in 't Zand 1992, for more detail). Background radiation is then automatically subtracted. We then extracted 2−28 keV spectra from the resulting imaging data. Burst time bins were defined such that the significance of the source (i.e., the photon flux divided by the standard deviation expected from all other photon sources) is at least 10. Experience shows that spectra are ill defined for lower significances. The X-ray spectrum of the persistent emission around the burst was determined from the whole observation in which the burst occurred (with an exposure time of 14.3 ks). This spectrum was subtracted from the burst emission in our time-resolved burst spectral analysis. The burst and persistent spectra were fit in the 2−28 keV band.

2.1.5. *HETE-2* FREGATE

One of the instruments onboard the High Energy Transient Explorer satellite (*HETE-2*; Ricker et al. 2003) that operated between 2000 and 2007, was the omnidirectional γ-ray spectrometer named French Gamma Telescope (FREGATE; Atteia et al. 2003). FREGATE consisted of 4 detectors, mounted in two pairs. It was sensitive in the 6−400 keV range, with a maximum effective area of 158 cm^2. The field of view was 70° (half-width at zero response, *HWZR*), but it had no imaging capacities. It provided continuous 128 channel energy spectra with 5 s time resolution (except in the beginning of the mission when it was 10 s), as well as continuous four-channel energy spectra with 0.164 s time resolution (0.327 s in the beginning).

A burst trigger occurred when there were two coincident 6σ or higher excesses on two of the FREGATE detectors within a time bin; this corresponds to an increase by 1.2 Crab or higher in 5.24 s for a burst observed on-axis in a source-free region. When this happened, 256 000 individual photons were time- and energy-tagged. FREGATE triggered 13 times on bursts coming from the direction of 4U 0614+091 (see Table 2). Three of them were weak and exhibited low signal to noise (on MJD 52 961, MJD 53 074 and MJD 53 740). The first two FREGATE events (MJD 51 944 and MJD 52 322) were already reported by Barraud (2002); they occurred when the Wide Field X-ray Monitor (WXM, imager onboard *HETE-2*, 2−25 keV; Shirasaki et al. 2003) was not operating. The remaining bursts were detected by the WXM, and some of these were also detected by the Soft X-ray Camera (SXC, CCD-based imager onboard *HETE-2*, 0.5−2 keV; Villasenor et al. 2003). The WXM and SXC, when operating, were able to get precise burst localizations (see, e.g., Suzuki et al. 2004). Two additional bursts were seen by the WXM, but FREGATE was not operating at those times (MJD 53 041 and MJD 54 101). Due to the anti-solar pointing of HETE-2, 4U 0614+091 was within the field-of-view of FREGATE during nearly 4 months every year. We estimate the total exposure on 4U 0614+091 from 2001 to 2006 to be about 194 days.

The extraction of burst spectra relies on a quadratic fit of the "background" (i.e., true background plus any emission from sources in the field of view) during tens of seconds before and after a burst in all the 128 energy channels. The availability of this simple background spectrum allows for the subtraction of the background channel by channel. We used the counts above the fitted background to build the count spectrum of the burst, which we then deconvolved using the response matrix constructed with the known gain and angular response of the detector. We performed the X-ray spectral fits to the integrated and time-resolved (10 s resolution for the burst on MJD 51 944, 5 s for the rest) burst emission in the well-calibrated 7−40 keV range. For several of the bursts we also extracted spectral information at a higher time resolution in a similar way.

2.1.6. *INTEGRAL* IBIS/ISGRI and JEM-X

One of the two main instruments onboard *INTEGRAL* (International Gamma-Ray Astrophysics Laboratory; Winkler et al. 2003; launched October 2002) is IBIS (Imager on Board the INTEGRAL Satellite; Ubertini et al. 2003). It comprises two detector planes that view the sky through a coded mask. The field of view is 29° × 29° (*FWZR*) and the angular resolution is 12′ (*FWHM*). We use data collected with one of its detectors: the INTEGRAL Soft Gamma-Ray Imager (ISGRI) which is sensitive in the ≃15 keV to 1 MeV range with a total effective area of about 2600 cm^2 (Lebrun et al. 2003).

One of the two supplementing monitors onboard *INTEGRAL* is the Joint European X-ray Monitor (JEM-X; Lund et al. 2003). JEM-X consists of 2 identical units, which are both sensitive in the 3−35 keV band. Most of the time only one unit is operating. The angular resolution is 3′ (*FWHM*); one single unit has a detector area of about 500 cm^2. The units have a circular view with diameter of about 13° (*FWZR*), i.e., narrower than ISGRI. In practice, the transmission of the collimator beyond an off-axis

Table 2. Burst and persistent emission properties for all bursts from 4U 0614+091.

MJD	Start time (UTC)	Δt (day)	$t_{\rm rise}$ (s)	$t_{\rm decay}$ (s)	$\chi^2_{\rm red}$ /d.o.f.	$F_{\rm peak}$ (10^{-8} erg s^{-1} cm^{-2})	$E_{\rm b}$ (10^{-8} erg cm^{-2})	τ (s)	$t_{\rm dur}$ (s)	Time span (MJD−50 000)	$\chi^2_{\rm red,pl}$ /d.o.f.	$\gamma_{\rm pl}$	$N_{\rm pl}$	$F_{\rm X,l}$ (10^{-8} erg s^{-1} cm^{-2})
OSO-8/GCSXE														
42 680	1975-09-25 22:48	–	7	32^{+6}_{-5}	0.7/73	≃3.3/≃0.8[e] [1]	≃24[e] [1]	≃30[e]	71	–	–	–	–	0.05–0.09[f] , 0.02–0.13[g] [2]
SAS-3														
42 820	1976-02-12 20:17	140	–	–	–	≳0.5[h] [3]	≳38[h] [3]	∼76	–	–	–	–	–	≲0.11[h] [2]
GRANAT/WATCH														
47 908	1990-01-17 17:42:28	5088	40	$23.0^{+4.2}_{-3.5}$	1.0/49	≃19	≃907	≃48	136	–	–	–	–	≲0.33[i] , ≲0.34[j] [4, 5]
EURECA/WATCH														
49 019	1993-02-01 06:27:39	1111	21	$15.2^{+2.9}_{-2.3}$	1.0/53	≃19	≃352	≃19	59	–	–	–	–	0.020 ± 0.008[k] , 0.09 ± 0.01[l]
49 035	1993-02-17 11:09:27	16	9	$11.7^{+2.7}_{-2.3}$	1.2/54	≃21	≃258	≃12	33	–	–	–	–	"
49 048	1993-03-02 14:15:27	13	18	$6.0^{+0.9}_{-0.8}$	0.9/53	≃28	≃493	≃18	54	–	–	–	–	"
RXTE/ASM														$F_{\rm X}$ $F_{\rm X,bol}$
50 200	1996-04-27 10:25:37	1152	3	$13.0^{+1.5}_{-2.0}$	0.7/8	$7.9^{+1.1}_{-0.9}$	100 ± 4	12.6 ± 1.7	28	198.90–200.44	0.04/1	1.96 ± 0.28	0.37 ± 0.12	$0.10^{+0.06}_{-0.03}$ $0.49^{+0.17}_{-0.14}$
51 164	1998-12-17 01:29:22	91	1	7.8 ± 0.5	1.1/64	23^{+9}_{-5}	207 ± 29	9 ± 3	19	1162.50–1164.06	0.04/1	2.27 ± 0.21	0.43 ± 0.12	$0.08^{+0.03}_{-0.02}$ $0.42^{+0.11}_{-0.12}$
53 441[b]	2005-03-12 16:52:59	367	–	7571^{+995}_{-819}	2.4/29	≳0.67 ± 0.04	≳5525	≃8194	–	3438.00–3441.50	0.2/1	2.06 ± 0.31	0.31 ± 0.09	$0.07^{+0.03}_{-0.02}$ $0.35^{+0.12}_{-0.10}$
53 476	2005-04-16 15:35:09	16	1	$11.0^{+1.9}_{-1.4}$	2.1/7	$13.0^{+1.8}_{-1.5}$	132 ± 6	10.2 ± 1.4	21	3475.00–3476.65	3.8/1	1.59 ± 0.37	0.11 ± 0.06	$0.05^{+0.04}_{-0.02}$ $0.35^{+0.17}_{-0.09}$
53 959	2006-08-12 19:00:54	189	1	8.0 ± 0.7	1.0/78	$8.4^{+1.3}_{-1.1}$	69 ± 4	8.2 ± 1.3	17	3959.80–3962.00	0.1/1	2.53 ± 0.41	0.62 ± 0.34	$0.08^{+0.05}_{-0.03}$ $0.63^{+0.41}_{-0.36}$
54 101[c]	2007-01-01 11:32:49	72	2	$5.1^{+1.2}_{-0.8}$	1.3/3	$23.6^{+4.5}_{-3.5}$	156 ± 12	6.6 ± 1.2	15	4099.50–4101.48	0.07/1	2.37 ± 0.33	0.41 ± 0.17	$0.06^{+0.04}_{-0.02}$ $0.39^{+0.21}_{-0.16}$
54 108	2007-01-08 18:10:51	7	1	$11.0^{+2.3}_{-1.8}$	1.0/57	28^{+192}_{-14}	≃400	≃14	29	4106.50–4108.76	2.31/1	2.12 ± 0.27	0.31 ± 0.11	$0.07^{+0.04}_{-0.02}$ $0.33^{+0.13}_{-0.12}$
BeppoSAX/WFC														
51 073	1998-09-17 07:51:37	873	3	$18.2^{+4.1}_{-3.1}$	1.0/89	4.1 ± 0.4	111 ± 5	27 ± 3	57	1073.03–1073.66	0.9/25	2.17 ± 0.07	0.47 ± 0.05	$0.09^{+0.02}_{-0.01}$ $0.48^{+0.06}_{-0.05}$
RXTE/PCA & HEXTE														
51 789	2000-09-01 21:21 – 02 01:20	625	–	Tail info only:		≳0.123 ± 0.002	≳149	≃1211	–	1786.50–1788.90	1.4/1	2.05 ± 0.22	0.31 ± 0.10	$0.07^{+0.04}_{-0.02}$ $0.36^{+0.14}_{-0.12}$
51 944	2001-02-04 21:52:42.8	155	0.005	Tail info only:		≳0.033 ± 0.003	≳69	≃2090	–	See *HETE-2*/FREGATE burst on MJD 51944				
HETE-2/FREGATE														
51 944	2001-02-04 21:52:44 [H1488]	155	70	39.7 ± 1.5	1.2/226	26.6 ± 0.6	3170 ± 43	119 ± 3	308	1943.00–1944.90	0.2/1	2.21 ± 0.12	0.38 ± 0.06	$0.07^{+0.02}_{-0.01}$ $0.38^{+0.06}_{-0.07}$
52 322	2002-02-17 12:40:04 [H1926]	378	137	89 ± 5	1.1/366	28.1 ± 1.7	6075 ± 145	216 ± 14	569	2321.00–2322.52	0.02/1	1.94 ± 0.24	0.24 ± 0.08	$0.07^{+0.04}_{-0.02}$ $0.32^{+0.13}_{-0.10}$
52 951	2003-11-08 16:23:18 [H2915]	84	8	6.7 ± 0.2	1.4/88	26.5 ± 0.5	493 ± 14	18.6 ± 0.6	45	2950.00–2951.68	1.8/1	1.91 ± 0.27	0.22 ± 0.10	$0.07^{+0.04}_{-0.02}$ $0.31^{+0.04}_{-0.02}$
52 961	2003-11-18 07:34:46 [H2935]	10	2	4.4 ± 0.8	0.9/97	≃12	80 ± 11	≃7	16	2959.50–2961.30	2.0/1	1.93 ± 0.19	0.31 ± 0.09	$0.09^{+0.04}_{-0.02}$ $0.43^{+0.16}_{-0.12}$
52 978	2003-12-05 23:03:43 [H2959]	78	5	20.4 ± 0.5	1.2/182	29.6 ± 0.5	1240 ± 21	42.0 ± 1.0	89	2977.00–2978.95	0.9/1	1.95 ± 0.31	0.19 ± 0.09	$0.05^{+0.03}_{-0.02}$ $0.26^{+0.14}_{-0.11}$
52 989	2003-12-16 19:34:07 [H2974]	11	5	6.7 ± 0.3	1.3/93	24.1 ± 0.5	318 ± 10	13.2 ± 0.5	31	2988.00–2989.81	0.1/1	2.20 ± 0.34	0.62 ± 0.30	$0.12^{+0.08}_{-0.04}$ $0.61^{+0.34}_{-0.31}$
52 997	2003-12-24 11:50:29 [H2980]	8	4	3.7 ± 0.2	1.4/94	24.0 ± 1.0	199 ± 8	8.3 ± 0.5	21	2997.50–2999.00	1.6/1	2.06 ± 0.14	0.68 ± 0.14	$0.16^{+0.05}_{-0.04}$ $0.76^{+0.20}_{-0.16}$
53 041[d]	2004-02-06 10:04:45 [H3040]	22	–	–	–	–	–	–	–	3040.00–3041.40	0.2/1	2.39 ± 0.48	0.35 ± 0.23	$0.05^{+0.04}_{-0.02}$ $0.34^{+0.27}_{-0.23}$
53 019	2004-01-15 21:28:27 [H3012]	22	4	9.6 ± 0.4	1.0/93	21.8 ± 0.5	389 ± 7	17.9 ± 0.5	40	3018.00–3019.88	0.4/1	1.97 ± 0.21	0.21 ± 0.07	$0.06^{+0.03}_{-0.02}$ $0.27^{+0.11}_{-0.08}$
53 074	2004-03-10 10:06:21 [H3103]	33	2	3.5 ± 0.7	0.8/68	≃29	113 ± 15	≃4	10	3072.50–3074.41	1.9/1	2.20 ± 0.19	0.32 ± 0.09	$0.06^{+0.03}_{-0.02}$ $0.32^{+0.07}_{-0.09}$
53 702	2005-11-28 21:27:17 [H3972]	226	8	14.2 ± 0.5	1.1/134	31.3 ± 0.6	1015 ± 16	32.4 ± 0.8	73	3699.00–3702.88	1.8/1	2.33 ± 0.45	0.44 ± 0.28	$0.05^{+0.04}_{-0.01}$ $0.38^{+0.17}_{-0.10}$
53 718	2005-12-14 18:45:31 [H3982]	16	11	11.3 ± 0.3	1.4/107	31.5 ± 0.5	805 ± 24	25.5 ± 0.9	62	3717.00–3718.77	0.1/1	1.95 ± 0.30	0.26 ± 0.11	$0.07^{+0.04}_{-0.02}$ $0.33^{+0.16}_{-0.13}$
53 740	2006-01-05 05:18:53 [H3994]	22	1	2.7 ± 0.7	0.8/73	≃8	27 ± 6	≃3	7	3738.50–3740.22	0.6/1	1.71 ± 0.38	0.16 ± 0.10	$0.06^{+0.04}_{-0.02}$ $0.37^{+0.19}_{-0.12}$
53 770	2006-02-04 17:48:46 [H4020]	30	2	10.9 ± 0.6	1.3/91	24.5 ± 0.8	525 ± 15	21.4 ± 0.9	45	3769.00–3770.74	0.1/1	1.62 ± 0.25	0.17 ± 0.06	$0.08^{+0.04}_{-0.02}$ $0.50^{+0.24}_{-0.11}$

Table 2. continued.

MJD	Start time (UTC)	Δt (day)	t_{rise} (s)	t_{decay} (s)	χ^2_{red} /d.o.f.	F_{peak} (10^{-8} erg s^{-1} cm^{-2})	E_b (10^{-8} erg cm^{-2})	τ (s)	t_{dur} (s)	Time span (MJD−50 000)	$\chi^2_{red,pl}$ /d.o.f.	γ_{pl}	N_{pl}	$F_{X,1}$ (10^{-8} erg s^{-1} cm^{-2})
INTEGRAL/IBIS/ISGRI														
52 867	2003-08-16 21:31:26	545	14	$4.3^{+1.4}_{-1.0}$	0.8/34	30 ± 4	179^{+81}_{-50}	≃6	26	2866.00–2867.89	0.01/1	2.16 ± 0.35	0.27 ± 0.15	$0.05^{+0.04}_{-0.02}$ $0.27^{+0.18}_{-0.15}$
53 460	2005-03-31 07:12:18 [2441]	19	5	$2.0^{+0.3}_{-0.2}$	0.3/38	11 ± 2	342^{+126}_{-85}	≃31	67	3455.00–3460.25	1.5/10	2.01 ± 0.10	0.18 ± 0.05	$0.05^{+0.01}_{-0.01}$ $0.22^{+0.04}_{-0.06}$
Swift/BAT														
54 029	2006-10-21 09:01:54 [234849]	70	14	6.4 ± 0.5	1.2/22	27^{+7}_{-5}	545 ± 49	20 ± 5	54	4028.00–4029.38	1.1/1	2.06 ± 0.23	0.34 ± 0.11	$0.08^{+0.04}_{-0.03}$ $0.38^{+0.13}_{-0.12}$
54 189	2007-03-30 08:53:15 [273106]	81	9	$3.2^{+0.5}_{-0.4}$	1.3/28	33^{+12}_{-8}	187 ± 65	6 ± 3	21	4189.00–4190.37	0.04/1	2.12 ± 0.16	0.46 ± 0.10	$0.10^{+0.03}_{-0.02}$ $0.49^{+0.12}_{-0.10}$

References. [1] Swank et al. (1978); [2] Mason et al. (1976); [3] Lewin (1976); [4] Kitamoto (priv. comm.); [5] Brandt et al. (1992); [6] http://space.mit.edu/HETE/Bursts/summaries.html.

Notes. The first 3 columns give the day of the burst, its start time (trigger numbers in brackets) and time since the last observed burst (Δt). For the burst parameters (t_{rise}, t_{decay}, F_{peak}, E_b, τ and t_{dur}) see Sect. 2.2.1; χ^2_{red}/d.o.f. gives the goodness of the fit of the decay to an exponential and the degrees of freedom (d.o.f.). The rest of the columns refer to the average ASM persistent emission (Sect. 2.2.2): time span over which it was averaged, goodness of fit of the emission to a power law and d.o.f. ($\chi^2_{red,pl}$/d.o.f.) and parameters γ_{pl} and N_{pl}. $F_{X,1}$, F_X and $F_{X,bol}$ refer to literature[a] values of the absorbed persistent flux in various energy bands before 1994[d−k], and the unabsorbed persistent fluxes at 2−10 keV and 0.1−200 keV after 1994, respectively. References are given between brackets, see above.
[b] Superburst; [c] also seen by *HETE-2*/WXM (H4087) [6]; [d] only seen by *HETE-2*/WXM [6]; [e] 2−20 keV; [f] 2−6 keV; [g] 2.5−7.5 keV; [h] 1.3−5 keV; [i] 1−20 keV; [j] 6−150 keV; [k] 6−12 keV; [l] 20−100 keV.

angle of 5° is so low that only the brightest sources can be observed at larger angles. JEM-X is sensitive to X-ray bursts seen on-axis down to about 0.1 Crab at the 5σ level in 5 s.

The INTEGRAL Burst Alert System (IBAS; Mereghetti et al. 2003)[5] is the automatic on-ground software that in near-real time searches for γ-ray bursts in IBIS data and promptly publicly distributes results. For a trigger time interval of 1 s and a certain threshold value (currently about 8σ), a minimum flux of about 0.5−0.75 Crab (20−200 keV) is required to trigger a typical γ-ray burst (and to produce enough counts to locate the position in the deconvolved image). One burst from 4U 0614+091 triggered IBAS on UT 2005 March 31 (nr. 2441 on MJD 53 460).

To search offline for bursts and to study the hard X-ray long-term persistent behaviour of 4U 0614+091, we analysed all public *INTEGRAL* pointing data in the ISOC Science Data Archive[6]. Up to September 2007 there were ≃840 pointings available where 4U 0614+091 was within the ISGRI field of view with a total exposure time of about 25 days. Since most of these observations were taken with the prime objective of instrument calibration on the Crab, many pointings (about 200) were carried out in non-standard modes. The total exposure time of all ISGRI standard pointings is about 22 days. All public JEM-X data whenever 4U 0614+091 was in the field of view (i.e., <6° off-axis) amounts to a total exposure of only about 70 ks. In our analysis we use the high-energy source ISDC reference catalog (see Ebisawa et al. 2003; v. 27) as input source catalog. We processed the ISGRI and JEM-X data using the latest available Off-line Scientific Analysis software (OSA; see Courvoisier et al. 2003), v. 7.0. The description of the algorithms used in the ISGRI and JEM-X scientific analyses can be found in Goldwurm et al. (2003) and Westergaard et al. (2003), respectively.

We 1) processed the ISGRI 15–20 keV band data using OSA with default parameters; 2) analysed the data through to the imaging step; and 3) extracted light curves for all detected sources with 10 s time resolution[7]. Next, a potential onset of a burst was flagged when, in a time bin, the difference between the source count rate and the average source count rate in the whole pointing exceeded four times the standard deviation of the count rates in the whole pointing. The count rate versus time was then examined around each flagged time to check for the presence of a shape consistent with that of a type I X-ray burst. If this was the case, we generated reconstructed images within the good-time interval covering the whole burst, and checked them visually to verify that the event indeed originated from 4U 0614+091.

Using the above described procedure we confirmed the burst which triggered IBAS in 2005 (see above). We also detected another burst from 4U 0614+091 on UT 2003 August 16 (MJD 52 867). Unfortunately, the latter burst was seen far off-axis, about 16.5°, near the edge of the detector (see Fig. A.3), and thus again outside the field of view of JEM-X. We found no bursts from 4U 0614+091 in the JEM-X data.

For the time-resolved spectral analysis of the 2005 burst we divided the burst only in three parts so that the rise, the top and the decay were covered with satisfactorily spectral quality, in 5 spectral energy bins covering 17 to 40 keV. The statistical quality of the 2003 burst precludes a time-resolved analysis. The ISGRI spectrum of the persistent emission around the 2005 burst is derived from the 1800 s single pointing during which the burst occurred. The net-burst spectra were calculated by subtracting

[5] http://ibas.iasf-milano.inaf.it/
[6] http://integral.esac.esa.int/isda/
[7] http://www.isdc.unige.ch/integral/download/osa_doc.

the persistent spectrum from the burst spectra. X-ray spectral fits to the burst and persistent ISGRI spectra were performed in the 17−40 keV and 20−200 keV bands, respectively. During the INTEGRAL observations around the 2003 burst 4U 0614+091 was always far off-axis (>10°), and therefore we did not include these ISGRI data in our analysis of the persistent emission.

For the long-term light curves we used OSA through the production of ISGRI images per single pointing in the 15−50 keV range. This energy band was chosen to supplement the ISGRI light curves with the publicly available BAT long-term light curves (see Sect. 2.1.7). We force the flux extraction of each of the catalog sources, regardless of the detection significance of the source (see, e.g., Kuulkers et al. 2007). The correction for off-axis response is generally good up to ≃10° from the centre of the field of view. We therefore selected only those pointings where 4U 0614+091 was less than 10° off axis. This led to a total of 115 pointings with different exposure times spanning the time interval from 2003 February 18 to 2006 April 18.

2.1.7. *Swift* BAT

The Burst Alert Telescope (BAT; Barthelmy et al. 2005) onboard *Swift* (launched November 2004; Gehrels et al. 2004) is a coded-aperture imager with a very wide field of view of about 2 steradians, which operates in the 15−150 keV band. The detector plane covers a net collecting area of 5200 cm^2; the BAT angular resolution is 22′ (*FWHM*).

As soon as the BAT triggers on a γ-ray burst, *Swift* automatically slews to the γ-ray burst position and starts to observe the source with its more sensitive instruments. However, strong type I X-ray bursts may also trigger the BAT (but do not lead to automatic slews if they come from a known source). Assuming a black-body source with $kT \simeq 2.5$ keV, the 5σ detection limit for the BAT in 5 s is approximately 0.7 Crab in the 15−25 keV band.

Two bursts from 4U 0614+091 triggered the BAT into a γ-ray burst data collecting mode but did not result in automated slews. The triggers occurred on UT 2006 October 21 (nr. 234849 on MJD 54 029) and 2007 March 31 (nr. 273106 on MJD 54 189). For these triggers, about 45 s of BAT event data were produced. A first account of these bursts has been given by Strohmayer et al. (2008). We ran the standard complete γ-ray burst processing script on the BAT burst products of the two triggers to obtain a first impression of the burst behaviour, and to derive an updated position of the origin of the burst (see Appendix A). We then applied the latest calibration available (as of August 2007) to these data (energy calibration, detector quality map, mask weighting), following the analysis threads provided by the *Swift* Science Center[8]. From these calibrated data we produced light curves, images and spectra. The first burst is strong enough to support a detailed time-resolved spectral analysis in the 15−30 keV band, starting with a time resolution of 1 s. For the second, weaker burst we started with a time resolution of 2 s. We doubled the spectral time bin size, whenever the net-burst rates following the peak decreased by a factor of $\sqrt{2}$.

The BAT continually monitors the sky; more than about 70% of the sky is observed on a daily basis. Results from this survey mode are publicly available in the form of light curves covering the 15−50 keV energy band on two time scales: a single Swift pointing (≃20 min) and the weighted average for each day[9]. In the latter a 6 mCrab source typically can be detected at the 3σ level (Krimm et al. 2006). We used the daily average light curve for 4U 0614+091 to study its long-term hard X-ray behaviour.

2.2. *Further data analysis issues*

2.2.1. X-ray burst properties

The band passes we used for the investigation of the burst light curves and extraction of some of the burst properties (see below) are 6−15 keV, 2−28 keV, 1.5−12 keV, 2−60 keV, 7−40 keV, and 15−30 keV for the *EURECA*/WATCH, WFC, ASM, PCA, FREGATE, and both the ISGRI and BAT, respectively.

For each of the ASM bursts, we derived the start time by taking the time when the count rate rose more than 5σ above the pre-burst level, while, for each FREGATE burst, the start time is the actual trigger time. For the other bursts we determined the start times by eye, because most of these bursts rise more slowly at higher energies. We define the burst rise time, $t_{\rm rise}$, as the difference between the time of the start and the time of the peak of the burst; the derived values were verified by visual inspection of the light curves. We estimate the error on the rise time to be about half a second (except during the spike of the burst observed on MJD 51 944, see Sect. 3.1.2). The decay times, $t_{\rm decay}$, are derived from fits of an exponential function plus a constant to the light curves. We fit from the maximum of the burst up to about 100 s after burst onset, if possible. For the longer bursts a longer time base was used when possible. When no post-burst information is available, we first fit the pre-burst rate with a constant and fix that when fitting the decay portion of the burst light curve. The range of values for which χ^2 remains within 1 of the minimum value (i.e., $\Delta\chi^2 = 1$) is used to set the uncertainties of the decay times (assuming the fit parameters are uncorrelated).

Further burst properties include the bolometric fluence ($E_{\rm b}$) and bolometric black-body peak flux ($F_{\rm peak}$), where the underlying assumption is that the burst emission is on top of unchanged persistent emission (see, e.g., Kuulkers et al. 2002b), as well as information on the out-of-burst, i.e., persistent, emission (see below). Estimates of $E_{\rm b}$ were obtained by integrating the fitted black-body models of the time-resolved spectra over photon energy and time (i.e., we do not take into account any residual burst emission outside the time range in which we did the time-resolved spectral fits). Since bursts decay more rapidly at higher energies, i.e., $t_{\rm decay}$ depends on the bandpass used, we also determine the characteristic decay time $\tau = E_{\rm b}/F_{\rm peak}$ which is not dependent on bandpass. Uncertainties in $E_{\rm b}$ and τ were estimated by propagating the errors derived from the individual time-resolved burst spectral fits and by assuming that these errors are symmetric. For the WATCH bursts and the 3 weak bursts observed by FREGATE, time-resolved X-ray spectral analysis is not possible. Instead, we derive $F_{\rm peak}$ from the peak count rates by scaling from the count rates and fluxes of the Crab. The Crab flux is taken to be 1.03×10^{-8} erg cm^{-2} s^{-1} in the 6−15 keV WATCH band and 1.89×10^{-8} erg cm^{-2} s^{-1} in the 7−40 keV FREGATE band. We then converted these values to estimated bolometric values assuming the emission comes from a 3 keV black body (which is fine for a large part of a burst seen at hard energies, see, e.g., Fig. 1). For the 3 weak FREGATE bursts we derived $E_{\rm b}$ from the average burst-integrated spectra; for the WATCH bursts we derived $E_{\rm b}$ from the burst integrated number

[8] http://swift.gsfc.nasa.gov/docs/swift/analysis/

[9] http://swift.gsfc.nasa.gov/docs/swift/results/transients/index.html

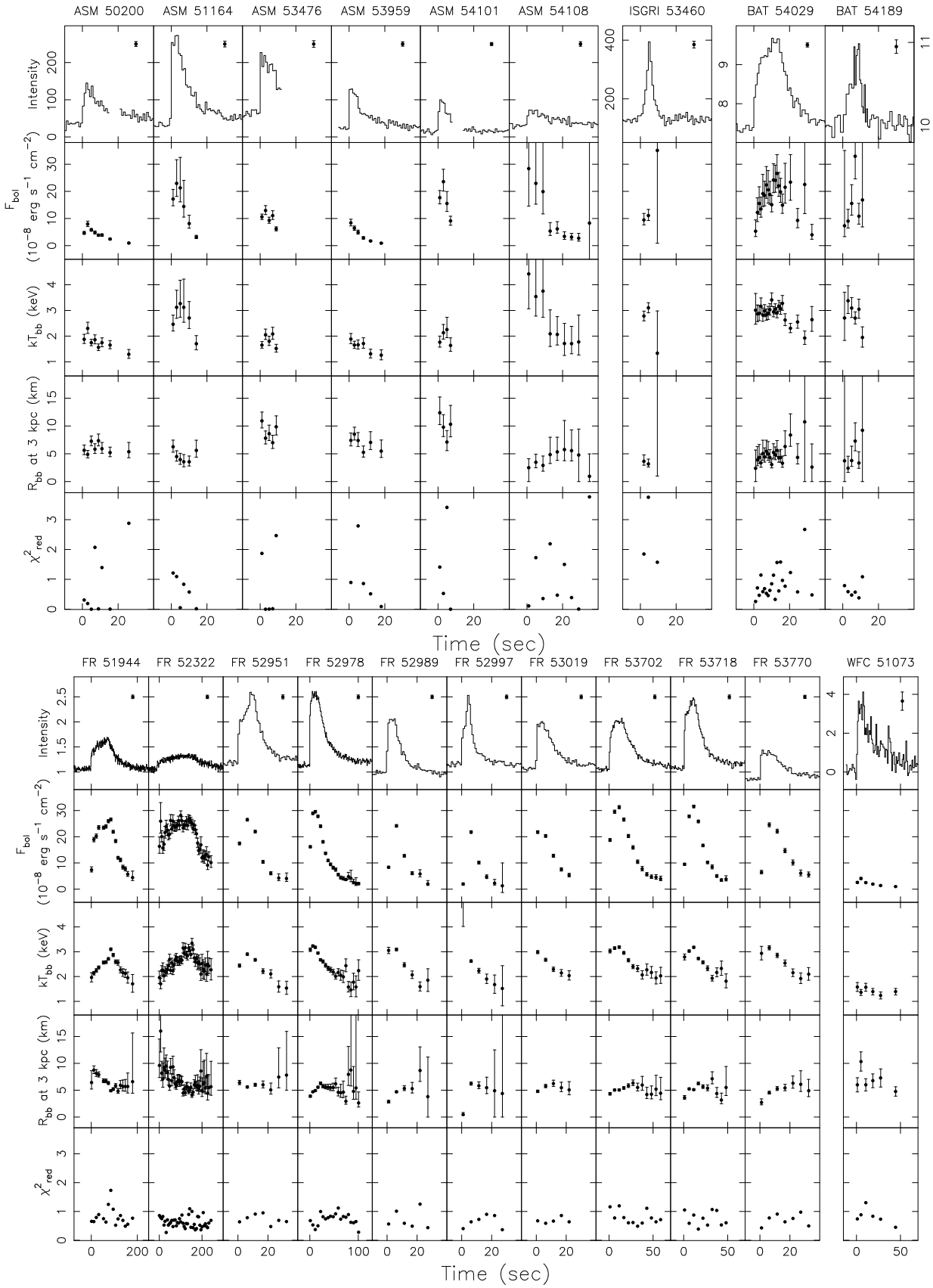

Fig. 1. Time profiles of raw full-bandpass photon rates (*top panels*), bolometric black-body flux (2nd panels), black-body temperature (3rd panels), black-body radius for 3 kpc distance (4th panels) and goodness of fit (*bottom panels*). The unit of intensity (*top panels*) is cts s^{-1} for the 6 ASM bursts, cts s^{-1} bin^{-1} for the ISGRI burst, kcts s^{-1} bin^{-1} for the 2 BAT bursts, kcts s^{-1} for the 10 FREGATE bursts and cts s^{-1} for the WFC burst. The bursts are denoted by instrument (FR = FREGATE) and MJD (see Table 2). For the ASM bursts which occurred on MJD 50 200 and MJD 51 164 we show the light curves from SSC1 and SSC0 data, respectively (see Table A.1).

of counts and by performing a correction similar to that described above for $F_{\rm peak}$. We define the duration of the burst ($t_{\rm dur}$) as $t_{\rm rise} + 2\tau$, since not all bursts are fully covered. Inspection of the light curves show that these values are consistent with the total durations determined by eye.

Burst oscillations at 414.7 Hz were present during a 5 s time interval in the brightest BAT burst cooling tail at the 4σ significance level (Strohmayer et al. 2008). We verified the presence of burst oscillations during this burst and searched for burst oscillations during the FREGATE and the 2005 ISGRI bursts where data were available at a high time resolution. We selected the 13−20 keV band for BAT, 15−30 keV for ISGRI and 7−40 keV for FREGATE, mainly to have the highest possible signal-to-noise ratio to search for a timing signature. We applied the Z_1^2-statistic (standard Rayleigh statistic, see Buccheri et al. 1983) to the photon event distributions for trial frequencies in a narrow window centred on the expected frequency of 414.7 Hz (i.e., 413−416 Hz). The dynamical power spectra were computed using the same method as in Strohmayer et al. (2008). We employed intervals of 4 s or 8 s, stepping through the BAT, FREGATE and ISGRI bursts with intervals of 0.25 s; for the calculation of upper limits we used intervals of 10 s.

We searched data from both the PCA and HEXTE for oscillations during the prompt burst seen on MJD 51 944 using fast Fourier transforms (FFTs). We used the single bit mode data available (full 2−60 keV PCA energy range taken at 122 μs time resolution). FFTs of data from 4 s-long intervals within the burst were performed keeping the original time resolution. For HEXTE we computed FFTs of 1 s-long sets of 15−40 keV band data with 122 μs time resolution. For the oscillation search in the long-lasting faint tails we employed the PCA data only.

2.2.2. X-ray spectral fits

In all our spectral fits (using XSPEC 11.3.0) we fix the low-energy absorption equivalent to a hydrogen column density of $N_{\rm H} = 3 \times 10^{21}$ cm^{-2} (e.g., Piraino et al. 1999; Méndez et al. 2002) for a composition of the absorbing matter as given by Wilms et al. (2000), employing absorption cross sections as provided by Verner et al. (1996). We derived errors in the fit parameters by using $\Delta\chi^2 = 1$ (assuming the fit parameters are uncorrelated). We use a distance of 3 kpc (see Sect. 3.1.2) when reporting black-body radii or emission areas, X-ray luminosities and absolute fluences.

To describe the persistent emission we used ASM spectra around the ASM, FREGATE, 2003 ISGRI and BAT bursts, ASM plus ISGRI spectra around the 2005 ISGRI burst and WFC spectra around the WFC burst. We also used PCA+HEXTE spectra, whenever available within about 1 day of a burst. All spectra, except the PCA+HEXTE spectra, could be well modelled by an absorbed power-law (power-law parameters: index, $\gamma_{\rm pl}$ and normalization at 1 keV, $N_{\rm pl}$). For the PCA+HEXTE spectral fits a soft component had to be included (we used a black body), as well as an Fe K line in the form of a Gaussian (line parameters: line energy, $E_{\rm Fe}$ (keV), and photon flux, $N_{\rm Fe}$ (photons cm^{-2} s^{-1}); line width arbitrarily fixed at 0.1 keV). The time ranges over which the persistent ASM or WFC emission was integrated are given in Table 2. For the ASM spectra we generally used all data from about 1.5 days before the burst up to the last dwell before the start of the burst. This leads to reasonably good spectra except for a few cases.

To get an estimate of the bolometric (unabsorbed) persistent luminosity, we extrapolate the spectral fit results to the 0.1−200 keV band (arbitrarily chosen). Note that these values should be taken with some caution: power-law emission can contribute significantly to the total spectrum, at the lowest energies for high power-spectral indices (about 80% and 8% of the 0.1−200 keV emission is at 0.1−2 keV and 10−200 keV, respectively, for $\gamma_{\rm pl} = 2.5$), and at the highest energies for low power-spectral indices (about 8% and 80%, respectively, for $\gamma_{\rm pl} = 1.5$).

XSPEC cannot provide errors on the integrated flux in an energy band. We therefore randomized the spectral parameters using the fit values and the derived 1σ-errors; this was done 10 000 times and we recorded the resulting integrated 2−10 keV and 0.1−200 keV fluxes. The flux distributions are significantly skewed towards larger fluxes. We therefore fitted the flux distributions below and above the peak of the distribution with Gaussians with different widths. The plus and minus errors in the integrated flux derived from the spectral fits were then taken as the 1σ widths.

2.3. Data and properties of previously reported bursts

We complete the information on the properties of the bursts seen after 1992 with that of the bursts reported by Lewin (1976), Swank et al. (1978) and Brandt et al. (1992). We digitized the 2−60 keV light curve of the *OSO-8*/GCXSE burst from Fig. 2 in Swank et al. (1978) and also obtained further information on the event from that paper. Data on the *GRANAT*/WATCH burst (6−20 keV; Brandt et al. 1992) is available in a form similar to that of the *EURECA*/WATCH bursts (see Sect. 2.1.1). We analysed this *GRANAT*/WATCH burst in a way similar to our analysis of the *EURECA*/WATCH bursts. Further information on the burst seen with the Horizontal Tube collimator (see Lewin et al. 1976) onboard SAS-3 was taken from Lewin (1976). Information about the persistent emission around the times of all these bursts, including those seen by *EURECA*/WATCH, were extracted from other literature (see Table 2).

3. Results

We report on 33 bursts from 4U 0614+091, including the bursts previously reported and the superburst. They are listed in Table 2. Figures 1 (top panels) and 2 present the raw light curves (for a perspective on the short time-scale behaviour of the bursts) of, respectively, 20 unpublished bursts, and the 3 previously reported *EURECA*/WATCH and the 2003 ISGRI bursts. Time-resolved spectroscopy for the 20 bursts is also presented separately in Fig. 1. An overview of the normal bursts is given in Sect. 3.1. The burst that occurred on MJD 51 944 and that shows evidence of radius expansion as well as a long-lasting faint tail is described in detail in Sect. 3.1.2. Our analysis of the superburst is presented in Sect. 3.2.

3.1. Overview of all normal bursts

Apart from the fact that 4U 0614+091 is not bursting as seldomly as previously thought, Table 2 shows that the recurrence time between bursts can be on the order of a week, when burst active (see also Sect. 3.5.1). The bursts generally last between about 10 s and 10 min (ignoring long-lasting faint tails, see below). Based on the FREGATE bursts, we designate bursts as short bursts if the burst duration is less than about 100 s, and intermediate-duration bursts if they last between about 5 and 10 min. The intermediate-duration bursts thus refer to the two bursts that were seen by FREGATE in 2001 and 2002. The

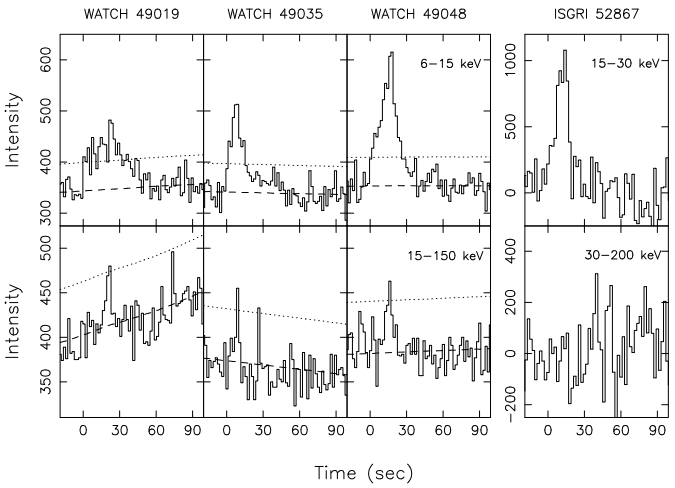

Fig. 2. *From left to right*: the 3 bursts observed with *EURECA*/WATCH in the 6−15 keV (*top*) and 15−150 keV (*bottom*) bands, and the burst observed with ISGRI in 2003 in the 15−30 keV (*top*) and 30−200 keV (*bottom*) bands. Zero time corresponds to the start of each burst (see Table 2). For *EURECA*/WATCH detector count rates (in cts bin^{-1}) are shown, i.e., no correction has been made for background and vignetting. The dashed line indicates the background level and the dotted line marks the 3σ excess level. For ISGRI the off-axis and background corrected count rates (in cts s^{-1}) are shown. The bursts are denoted by instrument and MJD (see Table 2).

short bursts will be discussed in Sect. 3.1.1 and the intermediate-duration bursts in Sect. 3.1.2.

Based on the facts that for all bursts the emission can be well described by black-body emission with canonical type I X-ray burst parameter values, that their profiles generally show an initial fast rise (at low energies) with a final slower decay which is exponential-like, and that the effective black-body temperature decreases during the decay for most of the bursts, we infer that the events are indeed type I X-ray bursts.

3.1.1. Short bursts

For the short bursts the rise times to maximum of the bursts as recorded by ASM, WFC and FREGATE are relatively fast, i.e., about 1−10 s. For the bursts seen by WATCH, ISGRI and BAT the rise times tend to be a bit longer, i.e., about 5−20 s; this can be attributed to these instruments being sensitive primarily at higher energies than the former instruments. Also, many of the bursts from these hard X-ray instruments show a two-stage rise, i.e., first a fast rise within seconds, then a slower rise to the peak intensity. The slow rise may be attributed to the slow increase in $kT_{\rm bb}$ (see, e.g., Fig. 1), and therefore to the peak of the X-ray spectrum shifting towards the centre of the instrument bandpass.

The short bursts have *e*-folding decay times between 2 and 20 s; the shortest decay times are seen at the highest energies (ISGRI and BAT), as expected if the burst spectrum softens during the decay. The characteristic decay time, τ, is in the range 6−42 s.

The WFC burst (on MJD 51 073) and two FREGATE bursts (on MJD 52 961 and MJD 53 740) are intrinsically weak; they reach peak intensities of less than a few Crab. The WFC event showed peak temperatures of about 1.5 keV, markedly below that seen during maximum of most of the other bursts (∼3 keV). These weak events may be similar to the burst reported from OSO-8, which reached a peak of ≃0.36 Crab and showed $kT_{\rm bb}$ = 0.8 ± 0.1 keV during the first 20 s (Swank et al. 1978; see also Table 2). The event seen by SAS-3 (Lewin 1976) was rather weak too (see Table 2), but only part of a burst was seen, so one cannot infer its true peak intensity.

The fluxes of the strongest bursts (including the intermediate-duration bursts) reach peak values of about 15 Crab. Both this and the properties of the time-resolved spectral fits (see Fig. 1 and Table 2) suggest they reach a limiting bolometric flux between about 21 and 32 × 10^{-8} erg cm^{-2} s^{-1}. When taking into account only those bursts which reached a peak flux of more than 15 × 10^{-8} erg cm^{-2} s^{-1}, the average peak value is about 27 × 10^{-8} erg cm^{-2} s^{-1} (fitting the observed values with a constant results, however, in a very high value of $\chi^2_{\rm red}$, i.e., 23, for 14 d.o.f.[10]). The highest bolometric peak flux measured is 31.5 ± 0.5 × 10^{-8} erg cm^{-2} s^{-1}.

The observed fluences, $E_{\rm b}$, of the intrinsically weak bursts are between 7 and 13 × 10^{-7} erg cm^{-2}. The values for the other short bursts range from about 16 to about 124 × 10^{-7} erg cm^{-2}. For a source distance of 3 kpc we derive absolute fluences from the above quoted values between 0.8 and 13 × 10^{39} erg.

We also inspected the burst light curves at higher time resolutions. One of the FREGATE bursts (MJD 52 997) showed an interesting spike at the start of the burst. The high-time resolution light curve is shown in Fig. 3 (top left). The spike lasts for about 0.3 s; after that the flux slowly rises to maximum for about 4 s. Double peaked light curves are typically seen in hard X-ray light curves when photospheric radius expansion is important (see, e.g., Lewin et al. 1984; Tawara et al. 1984; Cocchi et al. 2000). We performed time-resolved X-ray spectral fits at higher time resolution, to follow in more detail the evolution of the burst, especially the spike (Fig. 3, left, bottom panels). During the spike, the spectrum is quite hard compared to that generally observed near maximum of type I X-ray bursts ($kT_{\rm bb}$ = $4.3^{+0.6}_{-0.5}$ keV versus ≃3 keV), and $R_{\rm bb}$ is quite small. During the first few seconds $R_{\rm bb}$ rises, after which it drops slightly and then levels off. $kT_{\rm bb}$ quickly drops after the spike, but then it increases up to ≃3 keV at the peak of the burst. This may be a hint of a short radius-expansion phase, but the statistics are somewhat poor. Note that $F_{\rm bol}$ does not stay constant but slowly rises during that phase, casting some doubt on the radius-expansion interpretation.

3.1.2. Intermediate-duration bursts and evidence of photospheric radius expansion

The PCA light curve around the time of the start of burst MJD 51 944 is shown in Fig. 4. One may see a strong, very short, spike followed by a large drop in the flux, and then the onset of the main burst. In the top part of Fig. 3 (middle left), the first part of the burst is plotted again, but the spike is shown at higher time resolution. During the spike the intensity reaches maximum within 5 ms. Then, within 0.04 s, the intensity drops to a level consistent with the background and certainly below that seen before the spike. About 1.1 s later emission reappears again and continues as the main burst[11]. A local maximum is then reached within 2 s. In the spike, higher count rates are observed than during the first 30 s of the main burst.

The spike, drop below pre-burst levels and main burst indicate strong radius-expansion (see, e.g., Molkov et al. 2000; Strohmayer & Brown 2002; see also in 't Zand & Weinberg, in preparation). The results of the PCA time-resolved spectral

[10] The goodness of fit is expressed by the reduced chi-squared, or $\chi^2_{\rm red}$. It is the sum of the weighted square deviations between the data and the model, divided by the number of degrees of freedom (d.o.f.).

[11] FREGATE triggered on the main burst.

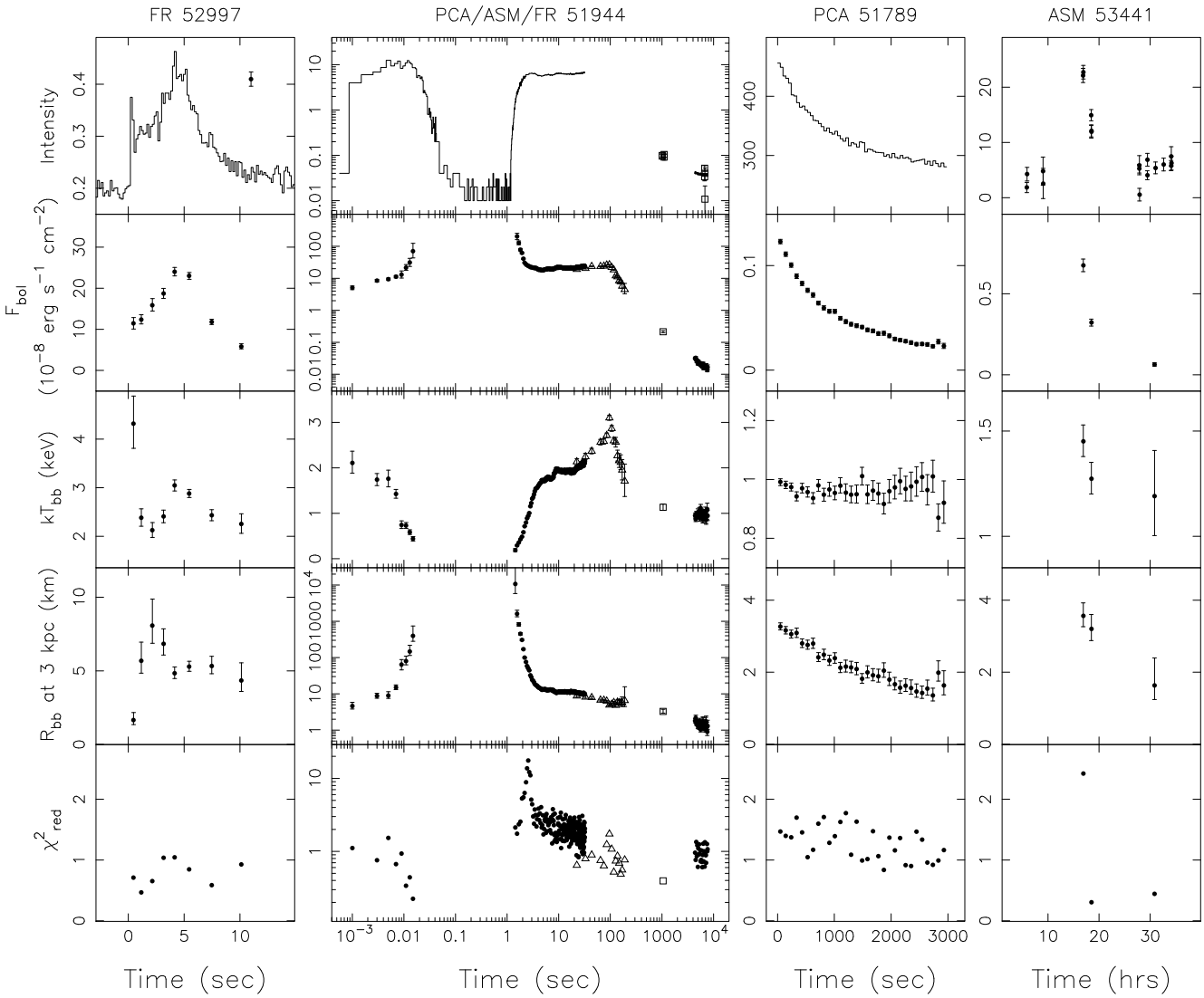

Fig. 3. Light curves (*top row*) and time-resolved spectral fit results (lower four rows) for selected bursts shown with higher time resolution than in Fig. 1. See the caption to Fig. 1 for brief explanations of the spectral parameters. The date (MJD) of each burst and the instrumental origin (FR = FREGATE) of the data are indicated. *Left*: FREGATE light curve and time-resolved spectroscopy for the burst on MJD 52 997 with a time resolution of 0.16 s. The unit of intensity is kcts s^{-1}. *Middle left*: (*top*) PCA full band-pass light curve of the MJD 51 944 burst with a time resolution of 0.001 s (from t = 0–0.05 s), 0.01 s (from t = 0.05–2.25 s), 0.125 s (from t = 2.25–30 s), and 16 s (from t = 4000–8000 s). The unit of intensity is 10^4 c s^{-1} per 4 PCUs. The PCA (PCU3) rates after t = 4000 s have been multiplied by four. The ASM data are indicated with open squares; they have been scaled to the PCA rates using the Crab as a reference. Time t = 0 s corresponds to UT 2001 Feb. 4 21:52:42.8. (rest) Time-resolved spectral fit results using the data from the PCA (filled circles), ASM (open squares) and FREGATE (open triangles). *Middle right*: PCA full band-pass light curve (*top*) and time resolved spectroscopy of the long-lasting faint tail of a possible burst observed on MJD 51 789. For this burst we do not have an exact start time, so t = 0 s corresponds to the start of the data sequence (UT 2000 Sep. 2 at 01:19:47). Intensity is in units of c s^{-1} for PCUs 2 and 3 combined. *Right*: ASM full-bandpass light curve of the superburst on MJD 53 441 from 4U 0614+091 (*top*) and time resolved spectroscopy. Time is given in hours since UT 2005 March 12, 0h, and the intensity is given in cts s^{-1}.

fits are shown in the bottom panels of Fig. 3 (middle left), together with spectral fits to the average of the ASM measurements about 0.3 h after the start of the burst. We also overlaid the spectral fit results from FREGATE (see Fig. 1, most left of bottom panels). Indeed, the inferred emitting area clearly increases during the spike and decreases during the very first part of the main burst. The expansion is more than 3 orders of magnitude. The peak of the emission (as parametrized by kT_{bb}) therefore shifts outside the PCA observable energy band, causing the dramatic drop in intensity.

After the fast contraction, it takes about 100 s for the burst to reach a maximum inferred temperature. During that time the emission area slowly decreases further (the end of this phase is usually referred to as "touch-down"). During the maximum of the main burst, between about 5 and 100 s after the start, the flux varies only slightly between about 18 and 26×10^{-8} erg s^{-1} cm^{-2}. This is consistent with the peak flux values reached during the other strong bursts (see Sect. 3.1.1). If we assume that during that time the flux is close to the Eddington value, the distance to the source may be inferred. By using the highest measured peak flux (Sect. 3.1.1) and the empirically derived Eddington luminosity of 3.79×10^{38} erg s^{-1} appropriate for a pure He accretor (Kuulkers et al. 2003), we infer a distance to the source of 3.2 kpc. Since the estimated uncertainty in the empirically derived Eddington luminosity is about 15% (see Kuulkers et al. 2003), we use for simplicity a distance

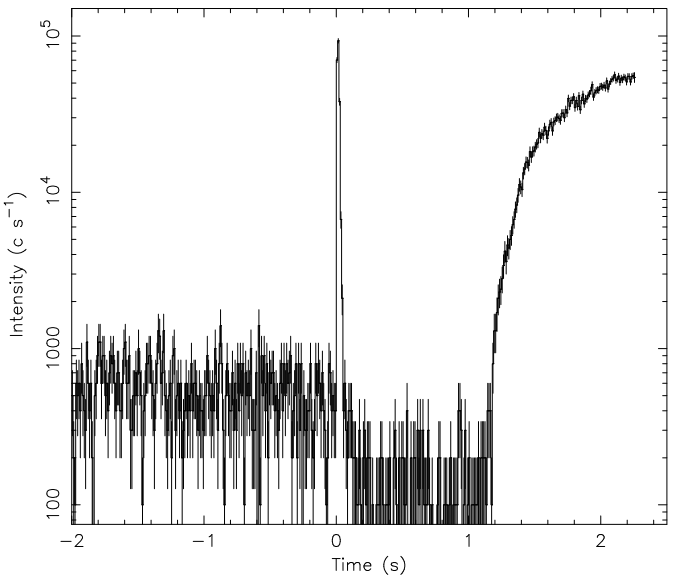

Fig. 4. PCA 2−60 keV light curve centred around the burst onset on MJD 51 944 at a 10 ms time resolution. The intensity is as measured by 4 PCUs combined. Time t = 0 s corresponds to UT 2001 Feb. 4 21:52:42.8.

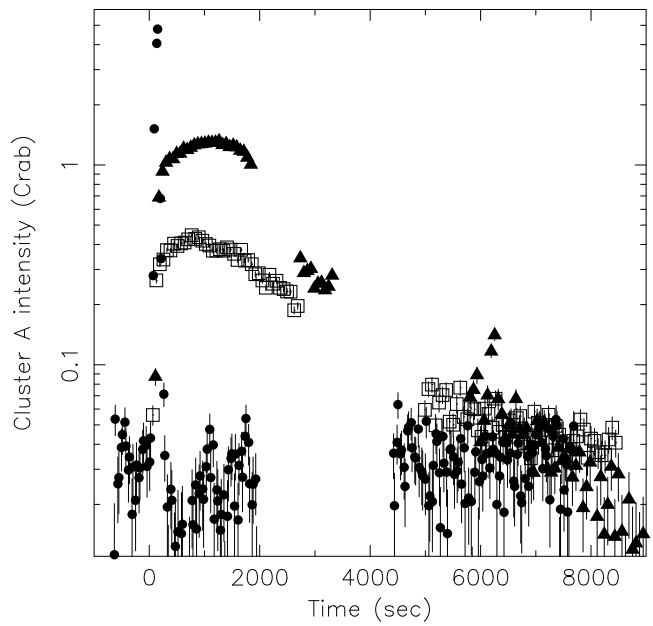

Fig. 5. HEXTE hard X-ray (15−60 keV, cluster A) light curve of the burst on MJD 51 944 of 4U 0614+091 (filled circles), as well as the superburst light curves of 4U 1820−303 (filled triangles) and 4U 1636−536 (open squares). The time resolution is 16 s for 4U 0614+091 and 32 s for 4U 1820−303 and 4U 1636−536. Time = 0 s corresponds to UT 2001-02-04 21:52:43, 1999-09-09 01:46:54 and 2001-02-22 16:52:11, for 4U 0614+091, 4U 1820−303 and 4U 1636−536, respectively.

value of 3 kpc in all our calculations. We note that during the strong expansion and contraction phase the apparent flux increases by more than an order of magnitude with respect to that described above. This would mean that super-Eddington fluxes are reached; however, since most of the emission is outside the PCA sensitive energy band and the spectra in this phase are highly non-Planckian (see below), these flux values must be regarded with caution.

Because of the very high count rates, the spectra constructed from the PCA data have small statistical errors, and this often means that simple spectral models are not sufficient to fit the spectra within the uncertainties. We find $\chi^2_{\rm red}$ values as high as 20, especially during the first part of the contraction phase (see bottom panel of Fig. 3, middle left). Deviations from a pure black body are seen frequently during radius-expansion bursts (see, e.g., Kuulkers et al. 2002b, 2003, and references therein). Since the temperature changes are fast during the expansion/contraction phase, a single black body may not be adequate in the time bins used. However, 10−20 s after the start of the bursts the temperature stays more or less constant, while still the spectra fits are not ideal. The deviations are thus intrinsic to the source.

Both intermediate-duration bursts show very long rise times during the main burst part, i.e., ≃70 s and ≃140 s, on MJD 51 944 and MJD 52 322, respectively. They also have long exponential and characteristic decay times, i.e., $t_{\rm decay} \simeq 40$ s and ≃90 s, respectively, and $\tau \simeq 119$ s and ≃216 s, respectively.

The burst on MJD 51 944 showed a long and faint tail, lasting for hours: after the main burst, during the next pass of PCA observations (between about 1.2 and 2.2 h after the start of the burst), the intensity was still slowly decaying but had not yet reached pre-burst levels. Serendipitously, the ASM scanned over 4U 0614+091 about 0.3 h (i.e., in between the two above described PCA passes) and 1.9 h after the start of the burst. The trend seen in the ASM data points is consistent with that seen in the second PCA pass (see Fig. 3, top middle left). The e-folding decay as measured from the bolometric black-body flux, $F_{\rm bol}$, light curves, $\tau_{\rm exp,bb}$, is 1143^{+2119}_{-492} s, i.e., a factor of about 35 longer than that measured during the first part of the decline from maximum of the main burst ($\tau_{\rm exp,bb} = 33^{+7}_{-5}$ s). During the first part of the decline $kT_{\rm bb}$ drops quickly (see Fig. 1), but after the flux has dropped by more than an order of magnitude, $kT_{\rm bb}$ does not decrease anymore, but stays more or less constant near 1 keV; the decrease in flux is then due to an inferred decrease in emitting area. About 5.2 h after the start of the burst the flux still had not yet reached pre-burst levels; the steady flux decay suggests that it is still due to remaining burst emission. However, at that low flux level we cannot be certain whether this is indeed remaining burst emission or due to a slight change in the persistent flux.

We found one other clear example of a long and faint tail in the PCA data, on MJD 51 789, between UT 01:19:34 and 02:10:35 (see Fig. 3, top, middle right). In the bottom panels of Fig. 3 (middle right) we show the results of the time-resolved fits. The behaviour is similar to that seen in the long-lasting faint tail of the burst on MJD 51 944, albeit at a slightly higher flux level: $kT_{\rm bb}$ stays constant near ≃1 keV, while the inferred emitting area decreases by a factor of about 2. The exponential decay time as measured from the bolometric black-body flux light curves is $\tau_{\rm exp,bb} = 868 \pm 32$ s. No *RXTE* observations of 4U 0614+091 were obtained for about 5 h prior to the start of the observation at UT 01:19:47 and none for about 2.5 h following the end of this observation. Therefore, an intermediate-duration burst like that seen on MJD 51 944 may have preceded the tail here.

Although the long-lasting faint tails last as long as various superbursts, their properties are different. Superbursts still show evidence of cooling, hours after they started. We show this in Fig. 5 by comparing the hard X-ray (15−60 keV) emission during the intermediate-duration burst with that seen during

the two superbursts observed from 4U 1820−303 (Strohmayer & Brown 2002) and 4U 1636−536 (Strohmayer & Markwardt 2002). Clearly, hard X-ray persists during most of the superburst, while it only lasts for minutes during the intermediate-duration burst.

For the two intermediate-duration bursts the observed fluences are approximately 320×10^{-7} erg cm^{-2} (MJD 51 944) and 610×10^{-7} erg cm^{-2} (MJD 52 322), corresponding to absolute fluences of 34×10^{39} erg s^{-1} and 67×10^{39} erg s^{-1}, respectively, at 3 kpc. We have ignored here any long-lasting faint tails; we expect that corrections for contributions from the tails would change the above values by only a few per cent (see Table 2).

3.2. Superburst

Inspection of the ASM light curve of 4U 0614+091 revealed a long flare on March 12, 2005 (MJD 53 441; see top right of Figs. 3 and 6, see also Kuulkers 2005). Between about UT 10:38 and 16:53 the ASM flux increased by a factor of 9.5 up to 0.3 Crab. About 1.5 h later the flux had dropped to 0.17 Crab; ≃9.5 h later it was still a factor of about 2 above the pre-flare flux level. The exponential decay time, $t_{\rm decay}$, of the flare is ≃2.1 h. We calculated the hardness ratio using various energy bands. We found the most significant results when we used the ratio of count rates in the 3−12 keV to 1.5−3 keV bands, as shown in Fig. 6. The hardness was higher during the flare than in the pre- or post-flare measurements; it softened during the decay. We investigated the raw dwell light curves during the flare, and found no evidence of strong variability, anomalous features such as normal bursts, or for instrumental artifacts. We, therefore, confidently attribute the high fluxes to the source.

We grouped the flare into three time bins, and performed a time-resolved spectral analysis of the average ASM spectra in these time bins. The spectra of the first two time bins are inconsistent with an absorbed power law ($\chi^2_{\rm red}$/d.o.f. of 6.1/1 and 16.2/1, respectively; for the third time bin $\chi^2_{\rm red}$/d.o.f. = 0.7/1). The net-flare spectra can best be modelled by absorbed black-body spectra. The results of this time resolved spectral analysis are displayed in Fig. 3 (right). The peak flux is rather low, about 0.7×10^{-8} erg s^{-1} cm^{-2}, and the maximum value for $kT_{\rm bb}$ black-body temperature only about 1.5 keV. However, we may not have seen the true peak intensity or black-body temperature due to the sparse coverage by the ASM. The inferred emission areas are rather low (2−4 km). They are similar to those inferred for the long-lasting faint tails of the bursts observed by the PCA (Sect. 3.1.2). However, $kT_{\rm bb}$ is somewhat higher, and the time scales involved about a factor of 7 longer, than those seen in these tails. Note that the inferred radii are not inconsistent with those seen during some of the superbursts from other LMXB burst sources (e.g., Kuulkers et al. 2002a). Since our observed flare resembles other superbursts, we suggest the flare to be a superburst.

3.3. Search for burst oscillations

We confirm the presence of burst oscillations during the brightest BAT burst, but do not detect any significant signal in any of the other bursts. This is no surprise: compared to the bright burst BAT light curve, the 2005 ISGRI burst light curve has a factor 6 lower signal-to-noise ratio, and the FREGATE light curves have a factor 1.6 to 2 lower signal-to-noise ratio. Therefore, a 4σ detection by BAT would correspond to non-detection by both ISGRI and FREGATE, assuming that the fractional amplitude was equal to that measured in the BAT data. We derive 3σ upper limits on the fractional rms (e.g., van der Klis 1995) in the 413−416 Hz range of about 4−6% at the peaks of the bursts observed by FREGATE, while they are about 9−12% in the burst tails.

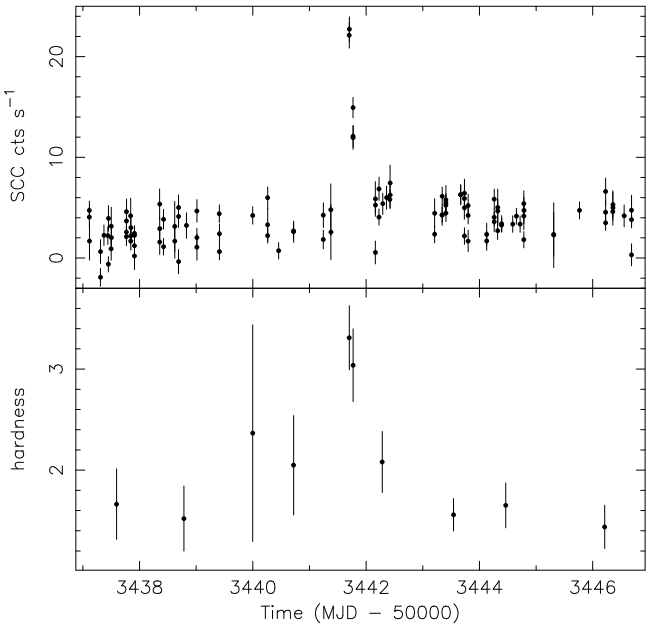

Fig. 6. ASM individual dwell intensity measurements (1.5−12 keV) and average hardness ratios around the time of the superburst from 4U 0614+091. Hardness is defined as the ratio of the intensity in the 3−12 keV band to that in the 1.5−3 keV band.

The 3σ upper limits on the fractional rms amplitude of burst oscillations during the prompt burst on MJD 51 944 are about 0.3% and 2% in the 100−1000 Hz range as measured by the PCA and HEXTE, respectively. Thus, if there were oscillations during the prompt burst on MJD 51 944 they were much weaker than those observed during the brightest BAT burst on MJD 54 029. No evidence of oscillations was found during the faint long-lasting tails either, with 3σ upper limits of about 1.2%.

3.4. Persistent emission

Moderate resolution X-ray spectra of the persistent emission from 4U 0614+091 above typically 1 keV have been satisfactorily fit by a soft component plus a hard, power-law component, both subjected to interstellar absorption. Generally, for 4U 0614+091 photon indices for the power-law component are found to be between 2 and 3 and temperatures for the soft black-body component are between kT = 0.5 and 1.5 keV. Total fluxes (1−20 keV) are typically between 1 and 5×10^{-9} erg s^{-1} cm^{-2} (Barret & Grindlay 1995; Ford et al. 1996, 1997; see also Piraino et al. 1999; Fiocchi et al. 2008). Our four most accurate measurements for these components are provided in Table 3. Our other lower-quality measurements based on power-law fits only are provided in Table 2. Our derived values of the power-law index, Γ, vary between ≃1.6 and ≃2.5. The persistent 2−10 keV flux is around $0.5–2 \times 10^{-9}$ erg s^{-1} cm^{-2}, with an average of $0.66 \pm 0.06 \times 10^{-9}$ erg s^{-1} cm^{-2}. Our spectral fits are consistent with that derived previously.

The unabsorbed bolometric flux (as estimated from the 0.1−200 keV flux estimates in Table 2, see Sect. 2.2.2) is about a factor of 5 higher than the 2−10 keV flux, i.e., on average $3.4 \pm 0.2 \times 10^{-9}$ erg s^{-1} cm^{-2}. The best estimates of the bolometric

Table 3. Results of spectral fits of PCA+HEXTE data taken outside of but within one day of bursts, i.e., representing persistent emission only.

MJD	Δt (days)	$\chi^2_{\rm red}$/d.o.f.	$kT_{\rm bb}$ (keV)	$R_{\rm bb}$ (km)	$F_{\rm bb,bol}$ (10^{-10} erg s^{-1} cm^{-2})	$\gamma_{\rm pl}$	$N_{\rm pl}$	$E_{\rm Fe}$ (keV)	$N_{\rm Fe}$ (10^{-3} ph s^{-1} cm^{-2})	$F_{\rm X}$ (10^{-10} erg s^{-1} cm^{-2})	$F_{\rm X,bol}$
51 789	<0.27	1.81/108	0.93 ± 0.01	1.45 ± 0.01	1.92 ± 0.03	1.841 ± 0.003	0.206 ± 0.001	6.9 ± 0.1	0.52 ± 0.05	8.37 ± 0.04	35.9 ± 0.2
51 944	0.09	1.17/108	1.02 ± 0.02	1.18 ± 0.01	1.75 ± 0.04	1.988 ± 0.004	0.289 ± 0.001	6.6 ± 0.1	0.58 ± 0.08	9.10 ± 0.06	37.7 ± 0.3
53 040	1.05	1.14/108	1.09 ± 0.01	1.12 ± 0.01	2.19 ± 0.04	2.162 ± 0.004	0.269 ± 0.002	6.8 ± 0.2	0.34 ± 0.11	7.36 ± 0.06	29.7 ± 0.2
54 188	1.02	1.35/79[a]	0.90 ± 0.02	1.51 ± 0.02	1.86 ± 0.04	1.957 ± 0.003	0.256 ± 0.001	6.7 ± 0.1	0.68 ± 0.07	8.44 ± 0.05	35.3 ± 0.2

Notes. [(a)] No HEXTE Cluster A spectrum.
Given are the day of the observation (MJD), the time to the closest burst (Δt), and the spectral parameter values. The latter are the goodness of fit degrees of freedom ($\chi^2_{\rm red}$/d.o.f.), the black-body parameters (temperature $kT_{\rm bb}$, radius $R_{\rm bb}$ at 3 kpc, bolometric black-body flux $F_{\rm bb,bol}$), the power-law parameters (power-law index $\gamma_{\rm pl}$, normalization at 1 keV $N_{\rm pl}$), the Gaussian line (presumably Fe K) parameters (line energy $E_{\rm Fe}$, line normalization $N_{\rm Fe}$; line width was fixed at 0.1 keV), and the unabsorbed fluxes in the 2−10 keV ($F_{\rm X}$) and 0.1−200 keV ($F_{\rm X,bol}$) bands.

correction factor from the 2−10 keV flux are obtained from a joint analysis of the PCA and HEXTE spectra, because of the quality and broad-band coverage. They are between 4.0 and 4.3 with an average of 4.16 ± 0.05 (see Table 3), which is consistent with that derived from the ASM plus ISGRI spectra (4.4 ± 1.3, see Table 2). These factors are compatible with that derived by in 't Zand et al. (2007) from a broad sample of LMXBs, i.e., a factor 2.9 ± 1.4 between the 2−10 keV flux and the bolometric flux as estimated from the extrapolated 0.1−100 keV flux, but are a bit higher than the value estimated by Migliari & Fender (2006) for an atoll source in the hard state, i.e., 2.5. Our bolometric fluxes derived from the ASM spectral fits are consistent with the fluxes derived from the broad-band PCA plus HEXTE spectral fits. Also, our fluxes are comparable to that measured using broad-band *BeppoSAX* data on 4U 0614+091 in the 0.1−200 keV band (Piraino et al. 1999; see also Fiocchi et al. 2008), as well as simultaneous *Swift*/XRT and PCA plus HEXTE data in the 0.6−100 keV band (Migliari et al. 2010). This lends confidence to the bolometric correction and the interpretation that the extrapolated 0.1−200 keV flux represents the bolometric flux.

If the source emits isotropically during and between bursts, and if the peak flux during the bursts $F_{\rm peak}$ represents emission at the Eddington limit, then the parameter γ ($\equiv F_{\rm pers}/F_{\rm peak}$, where both fluxes are bolometric) gives the source persistent luminosity in terms of the Eddington limit (see, e.g., Cornelisse et al. 2002b). Using the values from Table 2 and using only those bursts where $F_{\rm peak} > 15 \times 10^{-8}$ erg s^{-1} cm^{-2} (see Sect. 3.1.1), we find values for γ between about 0.0032 and 0.016, with an average of $\gamma = 0.013 \pm 0.001$. This is consistent with the estimates by, e.g., Ford et al. (2000) and in 't Zand et al. (2007).

3.5. Long-term X-ray behaviour

We investigated the long-term X-ray behaviour of 4U 0614+091 to see whether it affected its bursting behaviour using results from the *RXTE*/ASM (Sect. 3.5.1) and instruments on a number of other spacecrafts (Sect. 3.5.2).

3.5.1. ASM long-term persistent flux and burst recurrence times

The ASM data provide a uniquely long and homogeneous history of the persistent flux. In Fig. 7 (left) we show the ASM (1.5−12 keV) long-term light curves as daily averages. The corresponding average flux and variability (rms) per year are shown in Fig. 7 (right). From 1996 to mid 2000 the source was flaring on time scales of days to weeks from about 25−50 mCrab up to about 100−125 mCrab, with yearly averages above 30−35 mCrab. Then the source stayed at a relatively quiet level near 30 mCrab for about two and a half years (mid 2000 to 2003). Flaring behaviour similar to before mid 2000 was seen from 2003 to mid 2005. From mid 2005 to mid 2007 4U 0614+091 was still flaring, but less intensely, i.e., it varied from 25−50 mCrab up to about 75−100 mCrab and the yearly averages were again above 30−35 mCrab. The figure suggests that the degree of flaring and the long-term average (months to years) intensity seem to be related; a high degree of flaring is seen when the yearly average persistent flux is above about 30−35 mCrab and a low degree of flaring is seen otherwise. A flux of 30−35 mCrab (1.5−12 keV) corresponds to about 1% of the Eddington limit (see Sect. 3.4). For the following discussion we roughly divide the ASM history of 4U 0614+091 into three periods: (I) 1996−2000 flaring period, (II) 2001−2002 calm period, and (III) 2003−2007 flaring period.

In Fig. 7 (left) we mark the times of the normal bursts, as well as the superburst. The timing of burst detections is related, in part, to the times of year when the Sun is not near the source and the latter is more easily observed. Moreover, bursts could have occurred during many of the data gaps. It is also possible that with the ASM we missed the bursts which last significantly longer than the dwell duration (like the two intermediate-duration bursts). Also, weak bursts like that seen by the WFC may have been gone unnoticed with the other instruments; moreover, FREGATE, ISGRI and BAT operate in a higher bandpass than the ASM and WFC, and have to cope with higher backgrounds and so tend to trigger on brighter bursts. Therefore, we cannot rule out that we did not see all bursts which happened in our time frame of interest.

Figure 7 (left) suggests, however, that bursts appear more frequently during the 2003−2007 flaring period with respect to the previous periods. This is especially apparent if we take into account that during the 2000−2002 period there were 3 surveying X-ray instruments active (WFC, ASM and FREGATE). To support this suggestion, we determined the average burst recurrence times during the three above described periods for each instrument, as well as all together. We excluded results from the BAT (we only have information on triggered bursts, i.e., we did not perform a systematic search through the BAT archive) and JEM-X (very low source exposure time). We also did not take into account either the tail of a possible burst on MJD 51 789 or the superburst. When considering all instruments, we assumed that the exposure intervals did not overlap, and that they have the same efficiency in detecting bursts. We also assumed that the exposure time of a particular instrument is randomly distributed in each of the three periods. If n is the number of bursts seen during a certain period, then the average burst recurrence time is defined

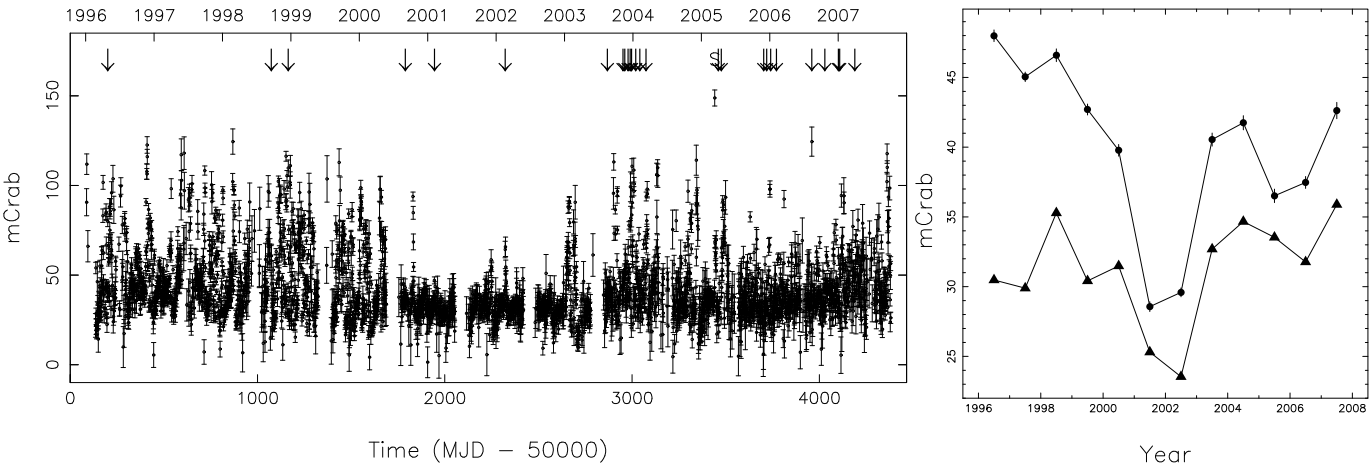

Fig. 7. *Left*: daily averaged ASM light curve (1.5−12 keV). The times of the normal bursts (see Table 2) are indicated with arrows at *the top*. The superburst occurrence is marked with an "S". *Right*: the yearly averaged ASM light curve (1.5−12 keV; filled circles) and the measure of the variability (rms) in the yearly time bins (filled triangles).

Table 4. Average burst recurrence time estimates for various instruments during three periods.

1996–2000 flaring period (I)				2001–2002 calm period (II)				2003–2007 flaring period (III)			
Inst	$t_{\rm exp}$ (d)	n^a	$\delta t_{\rm b}{}^b$ (d)	Inst	$t_{\rm exp}$ (d)	n	$\delta t_{\rm b}$ (d)	Inst	$t_{\rm exp}$ (d)	n	$\delta t_{\rm b}$ (d)
WFC	24.9	1	11–83	WFC	2.3	0	>5	WFC	–	–	–
ASM	27.5	2	7–31	ASM	9.6	0	>19	ASM	20.5	4	3–9
PCA	9.6	0	>19	PCA	3.7	1	2–12	PCA	9.4	0	>19
FREGATE	–	–	–	FREGATE	≃65	2	17–72	FREGATE	≃129	11	9–16
ISGRI	–	–	–	ISGRI	–	–	–	ISGRI	25.3	2	7–28
All	≃62	3	12–39	All	≃81	2^c	22–90	All	≃184	17	9–14

Notes. [(a)] n = number of bursts observed in the considered period; [(b)] $\delta t_{\rm b}$ = expected average burst recurrence time based on Poisson likelihood 1σ limits, see text; [(c)] Note that PCA and FREGATE observed one of the bursts simultaneously, see Sect. 3.1.2.

as $t_{\rm exp}$ divided by n, where $t_{\rm exp}$ is the total exposure time on the source in question in that period (note that this does not necessarily mean that the bursts recur periodically). Since we are dealing with relatively low number of observed bursts, Poisson statistics apply. For the expected range in average burst recurrence times ($\delta t_{\rm b}$) we use the Poisson likelihood 1σ lower and upper limits on the expected number of events when n events are observed (where $n = 0, 1, 2, 3, ...$). We verified our method by doing Monte Carlo simulations. The net source exposure times, number of bursts observed, and resulting average burst recurrence times per period of interest are shown in Table 4. For the individual instruments, the ASM and FREGATE give the best constraints on the average burst recurrence times, mainly because of the number of bursts observed. The estimates of the PCA average burst recurrence times differ significantly from those for the other instruments; we attribute this is to the fact that the data are not taken serendipitously, as well as to the relatively low exposure times.

The average burst recurrence times in periods I and II are not significantly different; the average over the two periods combined is 29^{+17}_{-10} days (taking into account all considered instruments). Period III shows a significant change in the average burst recurrence time with respect to the previous period: 11^{+3}_{-2} days (taking into account all considered instruments); it is just consistent with period I. The lower limit on the average burst recurrence time in period III is close to the shortest observed value of Δt in that period (7 days, see Table 2). During the EURECA/WATCH period in 1993 the burst average recurrence time is 17^{+15}_{-7} days, consistent with values of Δt in that period (see Table 2). It is consistent also with the values of all three ASM periods I−III.

Interestingly, the only two bursts that were observed in 2001 and 2002 are both intermediate-duration bursts. They thus occurred during a period when 4U 0614+091 was not only less burst active, but also when the persistent emission was rather calm and had the lowest averaged values. All other bursts (22, including the BAT bursts) are shorter and occurred during the two flaring periods. The burst duration, therefore, seems to be related to the level of the persistent emission, and possibly to the degree of flaring.

3.5.2. Further long-term broad-band X-ray behaviour

4U 0614+091 was discovered by *UHURU* with variable flux levels between about 15 and 70 mCrab (2−6 keV; Giacconi et al. 1972). Other early measurements of the flux, besides those from *UHURU*, may be found in, e.g., Mason et al. (1976), Swank et al. (1978), Parsignault & Grindlay (1978), Markert et al. (1979), and Warwick et al. (1981). In that time it was always seen at a flux of about 10−100 mCrab in roughly the ∼2 to ∼10 keV band. During sporadic measurements by the *Ginga*/All Sky Monitor between February 1987 and November 1991 4U 0614+091 was never detected in the 1−20 keV band, with an upper limit on the source flux of about 100 mCrab (S. Kitamoto, private communication).

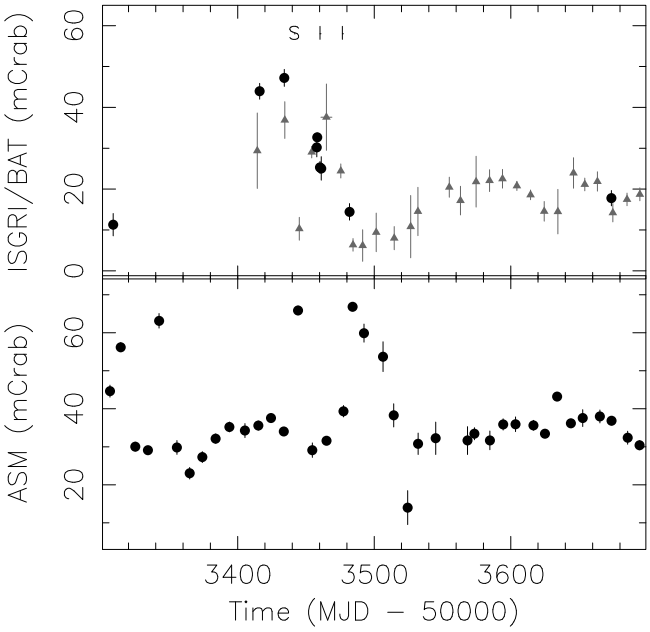

Fig. 8. Zoom in on the long-term hard X-ray (15−50 keV) light curve (*top*) and soft X-ray (1.5−12 keV) light curve (*bottom*), of 4U 0614+091. Shown are the 1-day and 10-day averages for ISGRI (filled circles) and *Swift*/BAT (grey filled triangles), respectively (*top*), and 10-day averages for the ASM. Time in years is given above the plot. The occurrence times of the normal bursts are indicated by arrows at *the top*. The superburst occurrence is marked with an "S".

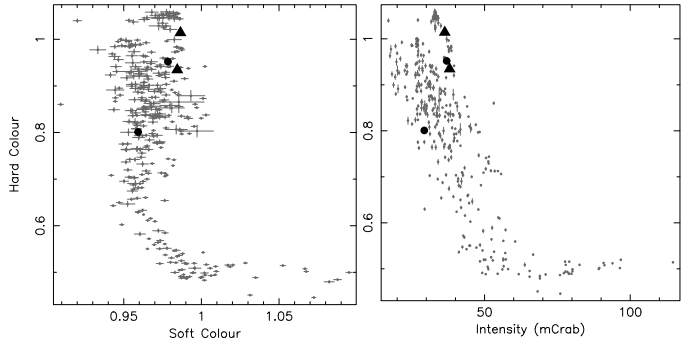

Fig. 9. PCA colour−colour diagram (*Left*) and hardness-intensity diagram (*Right*) of all public data of 4U 0614+091. Plotted are all persistent data points averaged per observation, and normalised using the Crab (see Sect. 2.1.3). Data taken close to a burst are marked with a black filled triangle ($\Delta t < 0.3$ days) or a black filled circle ($\Delta t \sim 1$ day). For the definitions of the colours and intensity, see Sect. 2.1.3.

4U 0614+091 was too weak to be detected by *EURECA*/WATCH on a daily basis, but data from the entire observation period can be combined. By adding the skymaps (see Brandt 1994, for a description of the technique), 4U 0614+091 was detected at an average persistent flux of 25 ± 10 mCrab in the 6−12 keV energy band (see also Fig. A.1, right).

We investigated the *CGRO*/BATSE occultation measurements (see, e.g., Harmon et al. 2004) in the period April 1991 and November 2000; they show 10-day average 20−100 keV fluxes from non-detections (with typical 10-day 3σ upper limits between about 50−70 mCrab) up to about 150 mCrab. During the period of the *EURECA*/WATCH observations when 4U 0614+091 was in the field of view, the 20−100 keV flux was on average 57 ± 6 mCrab; close to the time of the bursts seen by *EURECA*/WATCH it was around 100 mCrab.

The BAT and ISGRI 15−50 keV long-term light curves are consistent with each other. The 15−50 keV flux in the February 2003 to September 2007 time frame ranges from a few mCrab to 50 mCrab, but is most frequently around 20 mCrab. A zoom in on the 15−50 keV light curve and the corresponding part of the ASM light curve is shown in Fig. 8. Three interesting features may be seen in this figure. First, there is a rapid increase to about 50 mCrab for about a month, followed by a drop within weeks to about 10 mCrab at MJD 53 500. After about 2 months it goes back up again to the average level. Second, whenever the hard X-ray flux drops below roughly 10 mCrab, the soft X-ray intensity increases, up to a factor of 2 or so. Such an anti-correlation between soft and hard X-rays on these long time scales was previously discussed by Barret & Grindlay (1995) and Ford et al. (1996). On the other hand, hard X-ray flares are *not* accompanied by changes in the soft X-ray emission. Third, the superburst occurred around the time when the 15−50 keV flux was at its highest level (unfortunately no simultaneous BAT measurements exist at the time of the superburst). Just after the superburst the 10-day average 15−50 keV flux is low, while the 1.5−12 keV flux is at high levels. The ASM data show that this high average flux is not only due to the superburst itself, but also to a somewhat increased persistent level just after the superburst (see Fig. 6): before the superburst the 1.5−12 keV flux was 31 ± 1 mCrab, whereas for several days after the superburst it was at an elevated level of 53 ± 2 mCrab. About 10 days after the superburst it was back at the pre-superburst level. A normal burst (MJD 53 460) was seen only 19 days after the superburst (see Table 2); note that this is only slightly longer than the typical average burst recurrence time when 4U 0614+091 is burst active (see Sect. 3.5).

The CD and HID (Fig. 9) are qualitatively similar to those presented for the PCA data obtained in 1996−1998 by van Straaten et al. (2000). The colours often change on a daily time scale, as is typical for atoll sources (e.g., Hasinger & van der Klis 1989). For a wide range in hard colour, the soft colour does not change noticeably. Only near the lowest hard colours does the soft colour start to change; then there is an anti-correlation between hard and soft colour. When the hard colours are lowest, however, the soft colour changes are large while the hard colour changes are small. This is in line with the broad-band behaviour on longer time scales of the fluxes in the 1.5−12 keV and 15−50 keV bands described in the previous paragraph. In the HID higher intensities correspond to lower hard colours. Again, at the highest intensities (above about 50 mCrab), however, the hard colour changes only very little. The part of the diagram where the soft colour and intensity increases at constant hard colour (value of about 0.5) is referred to as the soft state or "banana" branch (see van Straaten et al. 2000). The rest is referred to as the intermediate state or "island" branch.

For 4 bursts (i.e., those that occurred on MJD 51 789, MJD 51 944, 53 040 and 54 188) we have information about the persistent emission within about 1 day of the burst (see Table 3). In Fig. 9 we indicate the position the persistent source was in at these times. All 4 bursts occurred when the persistent emission was hardest and when the intensity was below ≃40 mCrab, i.e., when the source was in the intermediate or hard state ("island" or extreme "island").

4. Discussion

4.1. Observational summary

We have expanded the number of observed bursts that can be attributed to 4U 0614+091 from a handful to 33. These include a superburst. Most of the newly-found bursts are localized within 1.′5 of the optical position of 4U 0614+091. This confirms the type I X-ray burster nature of this low-mass X-ray binary. We find a significant change in the average burst recurrence time in a decade of observations, i.e., from roughly a month before mid-2003 to about one to two weeks afterwards. When burst active, the bursts have peak luminosities of about 3×10^{38} erg s^{-1}, last for up to about a minute, and release energies of about 10^{39}–10^{40} erg. The larger set of bursts shows a wide variety of characteristics, with dynamic ranges of a factor of 40 in peak flux, 100 in duration, and 230 in absolute fluence.

We found three long-duration bursts. Two of them have initial decay time scales of about 100 s and resemble intermediate-duration bursts seen from other sources (thought to be due to deep He flashes; see in 't Zand et al. 2005; Cumming et al. 2006). The third has an initial decay time of about 8000 s, comparable to the decay times of superbursts (due to an even deeper C flash contained in the ocean of the NS envelope; see Cumming & Bildsten 2001; Strohmayer & Brown 2002). It lasts a factor of 10 longer than the longest known intermediate-duration burst (for example, see in 't Zand et al. 2007; Keek & in 't Zand 2009). Unfortunately, the coverage of this burst is incomplete. This prevents a measurement of the true peak flux and a check for the occurrence of radius expansion. The average burst recurrence time when the two intermediate-duration bursts were seen, is notably longer than when the shorter bursts were seen (40^{+49}_{-18} days during a two-year period versus 11^{+3}_{-2} days for other bursts in the subsequent 4.7-year period).

One of the intermediate-duration bursts shows clear signs of strong radius expansion within the first few seconds of the event. The flux seen at the end of this episode of radius expansion must correspond to a luminosity near the Eddington limit, and we thereby confirm the distance to be close to 3 kpc. The average accretion rate suggested by the broad-band non-burst flux is 0.32–1.6% of the Eddington rate.

The two intermediate-duration bursts occur in a two-year time interval when the accretion flux lacks the otherwise so typical flaring behaviour and is on average about 30% lower than at other times. Similar effects are seen in other (candidate) UCXBs. A calm component is present which changes on time scales of a year, while flaring occurs with a time scale of a week (see in 't Zand et al. 2007). Also, bursts are shorter when a source shows more flaring activity (e.g., A 1246−58; in 't Zand et al. 2008). Moreover, UCXBs accreting above 1% of the Eddington limit show burst recurrence times on the order of days; those accreting below 1% of the Eddington limit show recurrence times on the order of weeks (in 't Zand et al. 2007). In this respect it is interesting to note that during 4U 0614+091's high flux and flaring period it was detected in the radio (0.34 ± 0.02 mJy at 4.86 GHz), while it was not detected during the low flux and calm period (3σ upper limit of about 0.1 mJy at 4.86 GHz). This supports the existence of different states and suggests a connection between the radio and X-ray emission mechanisms (Migliari et al. 2010).

The wide range of peak fluxes is not unprecedented. Galloway et al. (2008) find that roughly 2% of bursts have bolometric peak fluxes less than 0.1 times the maximum for the same source. Three sources exhibit dynamic ranges in excess of 100: EXO 0748−676 (236 ± 36), 4U 1608−522 (446 ± 115), and 4U 1636−536 (151 ± 25), although it should be mentioned that the high value in the last source is due to a weak secondary burst in a double burst (excluding that diminishes the dynamic range to 23 ± 1). These three sources are not UCXBs, implying that the wide dynamic range in 4U 0614+091 is not necessarily due to extraordinary abundances of H, He, C or O.

We found two long-lasting faint tails wherein the flux decays exponentially with a time constant in the range of 1000 to 2000 s. One of them is the remainder of the intermediate-duration radius-expansion burst. The tail is seen clearly up to at least 2.5 h after the start of the burst, possibly even up to 5 h. During the tail no cooling is seen; the inferred temperature stays constant near about 1 keV, while the apparent emitting area decreases. Similar faint tails have been seen in various other bursters (Linares et al. 2009; Falanga et al. 2009; in 't Zand et al. 2009), but they were not as long lasting as those seen in 4U 0614+091. A hot underlying neutron star (with temperatures between 0.5–1 keV, i.e., slightly lower than that found in the burst tail) can explain the fact that in the tails the inferred temperatures are effectively constant (van Paradijs & Lewin 1986; in 't Zand et al. 2009). In this regard, we note that a soft component in our persistent PCA spectral fits is present, perhaps coming from the neutron star and/or the inner parts of the accretion disk; when the soft component is modelled by a black-body we infer temperatures of about 1 keV, i.e., close to that found in the long-lasting tails. As noted by in 't Zand et al. (2009), neutron stars in UCXBs accrete at lower rates and lack the CNO burning of H in their surface layers, compared to those in other, ordinary, bursters. This may result in a cooler neutron star in the former systems, leading to a different behaviour in the long-lasting tails during their bursts. However, the temperature reached in the long-lasting faint tail of 4U 0614+091 (and that of the transient XTE J1701−407, see Linares et al. 2009; Falanga et al. 2009, presumably also containing a cool neutron star due to its long off-states) is similar to that seen in ordinary persistent bursters, which may indicate that a different explanation is required for the constant temperature in the tail.

4.2. The burst light curves and energetics

In an attempt to constrain the energy release and ignition depth of the bursts, we made some models of the light curves following the approach of Cumming & Macbeth (2004) for superbursts. We deposit an energy per unit mass $E = E_{17} \times 10^{17}$ erg g^{-1} uniformly in the layer down to a particular column depth y. The cooling of the layer is then followed by integrating the thermal diffusion equation. We set the composition after burning to be ^{56}Fe. Our models assume neutron star parameters of 1.4 $M_\odot$, $R = 10$ km, giving a redshift factor $1 + z = 1.31$ and $g = 2.44 \times 10^{14}$ cm s^{-2}. To avoid following the expansion of the outer layers that occurs when the luminosity approaches the Eddington limit, we set the top of our grid to $y = 10^8$ g cm^{-2}, and choose our outer boundary condition such that the maximum flux at that point is the Eddington flux at the surface of the star for pure He composition, i.e., $F_{\rm Edd} = cg/\kappa$ with $\kappa = 0.2$ cm^2 g^{-1} (Thomson scattering for pure He), giving $F_{\rm Edd,\infty} = F_{\rm Edd}/(1+z)^2 = 2.1 \times 10^{25}$ erg cm^{-2} s^{-1}. Because of this crude treatment of the outer layers, and the simplistic way in which the energy is initially deposited, our models are not valid for early times, $\lesssim$10 s (the thermal time scale at a depth of 10^8 g cm^{-2}).

We varied the two parameters E_{17} and y to find values that agree well with the observed light curves. Note that the values of E_{17} and y are taken to be independent parameters of

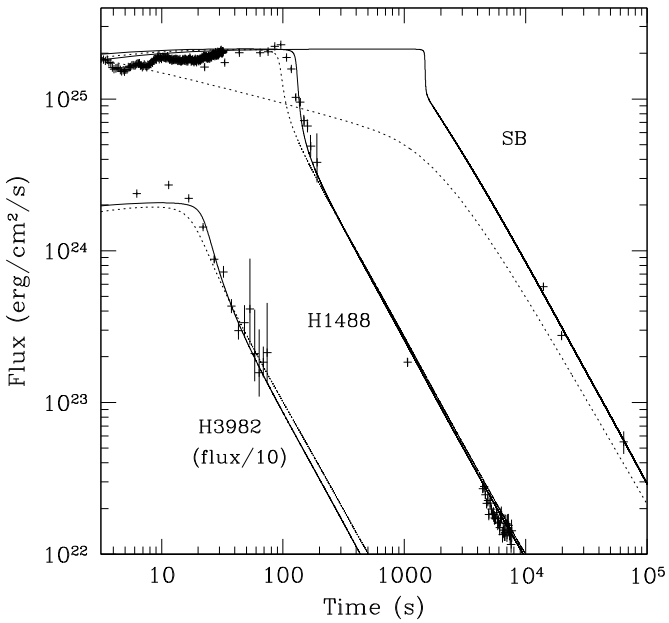

Fig. 10. Models of the burst light curves for the superburst (SB), the intermediate-duration burst on MJD 51 944 (H1488), and the short burst on MJD 53 718 (H3982). For the superburst, the model parameters are $E_{17} = 5$, $y_{11} = 2$ (solid curve) and $E_{17} = 2$, $y_{11} = 3$ (dotted curve). For the intermediate-duration burst, the model parameters are $E_{17} = 7$, $y_9 = 8$ (solid curve) and $E_{17} = 5$, $y_9 = 10$ (dotted curve). For the short burst, the model parameters are $E_{17} = 6$, $y_9 = 2$ (solid curve) and $E_{17} = 4$, $y_9 = 3$ (dotted curve). Here $E = E_{17} \times 10^{17}$ erg g^{-1} and $y = y_9 \times 10^9$ g cm^{-2} $= y_{11} \times 10^{11}$ g cm^{-2}. The observed fluxes and model fluxes for the short burst have been divided by a factor of ten for clarity. The start time of the superburst is unknown, but we find that choosing the start time to be around 4 h before the time of the first data point gives a slope for the observed light curve that agrees with the models. Here we adopt a start time of 3.9 h before the first data point.

the model, which allows us to investigate the ignition depth and energy release without assuming a particular fuel for the burst. The model light curves are compared with the observed light curves for the superburst, the intermediate-duration burst on MJD 51 944, and the short burst on MJD 53 718, in Fig. 10. We assume a distance to the source of $d = 3$ kpc and a neutron star radius $R = 10$ km to convert the observed fluxes into flux at the surface of the neutron star; these values give good agreement with the maximum flux from the model.

The best fitting column depths for the three bursts in order of decreasing duration are $y \simeq 2 \times 10^{11}$ g cm^{-2}, $\simeq 8 \times 10^9$ g cm^{-2}, and $\simeq 2 \times 10^9$ g cm^{-2}. For the intermediate-duration and short bursts, the column depths inferred from the light curves are consistent with accretion at about 1% Eddington for the observed times since the previous burst, $\Delta t = 155$ and 16 days, respectively (see Table 2). This can be derived as follows. The local Eddington accretion rate (accretion rate per unit area) at the surface of the neutron star is $\dot{m}_{\rm Edd} = c/R\kappa$. We define the Eddington rate as the value corresponding to $R = 10$ km and $\kappa = 0.2$ cm^2 g^{-1}, giving $\dot{m}_{\rm Edd} \equiv 1.5 \times 10^5$ g cm^{-2} s^{-1}, or $1\% \dot{m}_{\rm Edd} = 1500$ g cm^{-2} s^{-1}. Accretion at $\dot{m} = 1\% \dot{m}_{\rm Edd}$ then gives a column $y = \dot{m}\Delta t/(1+z) = 1.6 \times 10^9$ g cm^{-2} $(\Delta t/16$ d$)(\dot{m}/1\%\ \dot{m}_{\rm Edd})$. Matching the column depths inferred from the light curves assuming that Δt is the recurrence time implies $\dot{m} = 0.52\%$, and $1.3\% \dot{m}_{\rm Edd}$ for the intermediate-duration and short burst, respectively.

The time span between the superburst and the previous observed burst is 367 days (i.e., $\Delta t = 367$ days, see Table 2), in which time the accumulated column is $y = \dot{m}\Delta t/(1+z) = 3.7 \times 10^{10}$ g cm^{-2} $(\Delta t/367$ d$)(\dot{m}/1\% \dot{m}_{\rm Edd})$. Therefore, we require the accretion rate to be $\dot{m} \simeq 5\% \dot{m}_{\rm Edd}$ for the column inferred from the superburst light curve to be accreted in the 367 days leading up to the superburst (assuming no bursts occurred in between). An alternative explanation is that the superburst involves a different fuel layer (e.g., He for the short and intermediate-duration bursts, C for the superburst) in which case the column for the superburst could accumulate over a longer time scale than Δt. At 1% Eddington, the accumulation time would then be about 5 yr.

The best fitting values for the energy release are $E_{17} \approx 5$–7 (see Fig. 10). In addition, the fact that the light curves reach the Eddington flux implies a minimum energy release. For the intermediate-duration burst, we find that the flux does not reach the Eddington flux for $E_{17} \lesssim 4$. These values of energy release are smaller than the values $E_{17} \approx 16$ for complete burning of He to Fe group or $E_{17} \approx 10$ for complete burning of C to Fe group. This implies that the energy release is about a factor of 3 lower than expected for complete burning of pure He.

The low energies of the bursts can also be seen in the overall energetics. If all the matter accreted since the previous burst were completely burned during each burst, one would expect the ratio, α, of the average luminosity in the persistent emission to the time-averaged luminosity emitted in type-I X-ray bursts to have a value in the range 25–200, depending on the composition of the burning material. If one assumes that both the persistent and burst emission are isotropic, that the persistent emission has not varied since the previous burst, and that $F_{\rm pers}$ is the bolometric persistent flux, then this statement relating the persistent and burst luminosities is equivalent to $\alpha \equiv \Delta t F_{\rm pers}/E_{\rm b}$. If we take that the minimum average burst recurrence time is the lowest observed value for Δt, i.e., 7 days, then the corresponding values for α are in fact lower limits, which are between 125 and 5525 for the short bursts and around 30–70 for the intermediate-duration bursts. Calculating an α value by assuming that no bursts were missed between observed bursts (that is Δt is the average burst recurrence time) gives a range from 500 to 5000, larger than the canonical value of 100–200 for pure He burning. Another way to look at this is presented in Fig. 11 which shows the burst energy against time since the last burst Δt from Table 2. The solid lines show the expected burst energy as a function of recurrence time for accretion at 1% of the Eddington rate, for two different values of the nuclear energy release per nucleon $Q_{\rm nuc} = 1.6$ and 0.6 MeV per nucleon (where $E_{17} \sim 10(Q_{\rm nuc}/{\rm MeV}$ per nucleon$)$). The curves at the top left are pure He ignition models from Cumming et al. (2006) that assume complete burning. The observed bursts lie well below the expected energies assuming complete burning.

Figure 10 shows also that for the intermediate-duration burst on MJD 51 944, the model light curve nicely connects the early decay from the peak luminosity to the long tail lasting thousands of seconds. Therefore the long tail is naturally explained by the cooling of deep layers heated by the burst as proposed for tails seen in other sources by in 't Zand et al. (2009). The theoretical expectation is that the luminosity should decay as a power law in the cooling tail. This is confirmed by our observations (e.g., Fig. 10).

4.3. He as a fuel for the bursts

In Sect. 4.2, we found that the short and intermediate-duration burst light curves could be explained by ignition depths of $y \simeq 2$ and 8×10^9 g cm^{-2}, respectively, and that these depths are

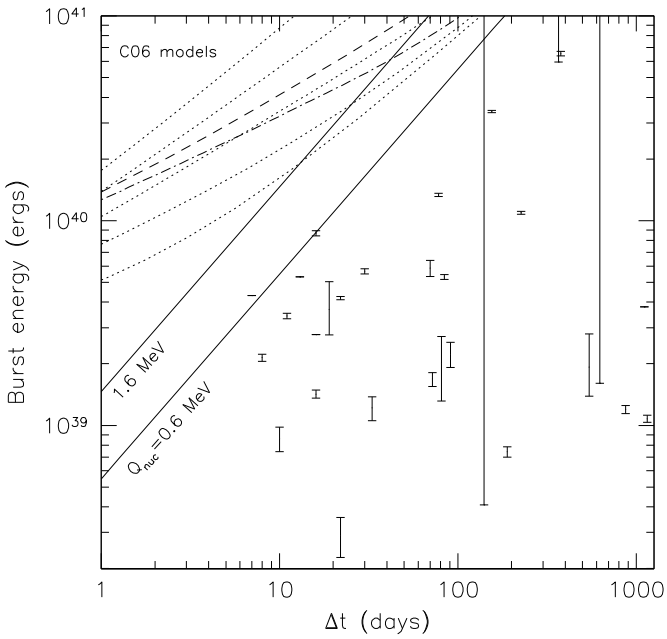

Fig. 11. The observed burst energies (assuming $d = 3$ kpc) versus the time since the last observed burst Δt from Table 2. Because of possible missed bursts due to the many data gaps, Δt is an upper limit on the average burst recurrence time. The solid lines show the expected relation for accretion at 1% of the Eddington rate assuming complete burning of the accumulated fuel for two different values of nuclear energy release per nucleon, $Q_{\rm nuc} = 1.6$ MeV corresponding to complete burning of pure He to Fe group, and a smaller value $Q_{\rm nuc} = 0.6$ MeV. The dotted, dashed, and dot-dashed curves show the predicted relation for pure He accretion from Cumming et al. (2006). (The different curves are for different core neutrino emissivities and crust properties; see Cumming et al. 2006, for details.)

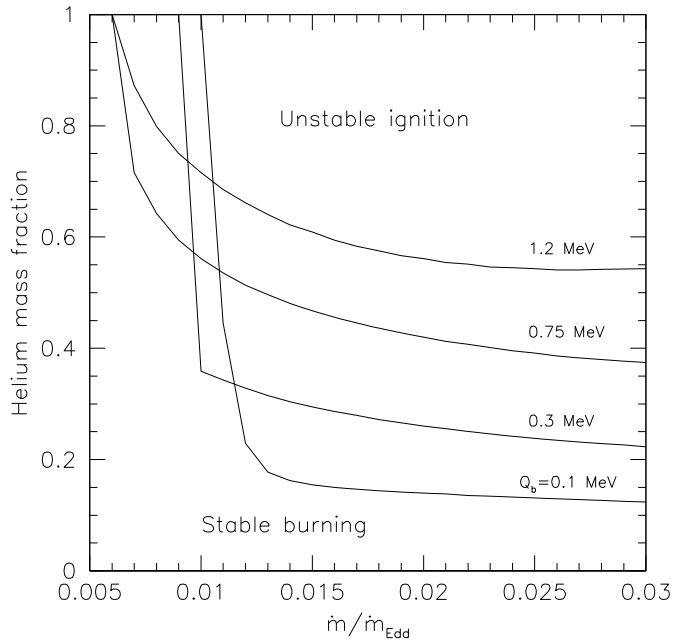

Fig. 12. The mass fraction of He needed to achieve unstable He ignition as a function of accretion rate, for accretion of He and an equal mixture of C and O. The different curves are for different values of $Q_{\rm b}$ as labeled.

compatible with the amount of mass accreted at an accretion rate close to $\dot{m} \simeq 1\%\ \dot{m}_{\rm Edd}$ in the observed time between bursts, Δt. These ignition depths would be naturally explained if the neutron star accreted a substantial amount of He. At low accretion rates, most of the energy released by pycnonuclear and electron capture reactions in the crust flows outwards, because the neutron star core is too cold for significant neutrino emission. This results in an outward flux from the crust of $F = \dot{m} Q_{\rm b}$ with $Q_{\rm b} \approx 1$ MeV per nucleon (Brown 2000; Cumming et al. 2006: their Fig. 18, top panel). For this value of $Q_{\rm b}$, Fig. 22 of Cumming et al. (2006) shows that pure He accretion gives ignition at $y \sim 10^9$–10^{10} g cm^{-2} at $\dot{m} \sim 1\%\ \dot{m}_{\rm Edd}$.

However, as we noted in the introduction, the lack of He lines in the optical spectrum of the source implies that the accreted material is not significantly enriched in He. To investigate whether a small amount of He in the accreted material could still explain the observed bursts, we constructed ignition models for type I X-ray bursts following Cumming & Bildsten (2000). We assume that the accreted material consists of He and a 50/50 C–O mixture. We find that for small He mass fractions, the He burns away stably before reaching the conditions required for a thermal runaway. In Fig. 12 we plot the He mass fraction required to achieve unstable ignition as a function of $\dot{m}$ and $Q_{\rm b}$. It shows that the amount of He inferred from the fits of disk spectra by Werner et al. (2006), i.e., $Y \lesssim 10\%$, do not lead to unstable ignition at any accretion rate unless the neutron star is cold, $Q_{\rm b} \ll 0.1$ MeV per nucleon, and even then the recurrence times are extremely long. We, therefore, conclude that matching the observations requires a significant amount of He in the accreted material.

If we allow a large enough He fraction, we can match the inferred ignition depth for the short and intermediate-duration bursts. For example, taking a He mass fraction $Y = 0.5$, $Q_{\rm b} = 0.3$ MeV per nucleon, and local accretion rates $\dot{m} = 3000$ and 5000 g cm^{-2} s^{-1} (2% and 3.3% of the Eddington rate) gives ignition depths of $y = 2$ and 8×10^9 g cm^{-2}, respectively. The corresponding recurrence times are 7 days and 46 days, respectively. For pure He and $Q_{\rm b} = 1$ MeV per nucleon, the correct ignition depths are obtained for $\dot{m} = 1\%$ and $1.7\%\ \dot{m}_{\rm Edd}$, with recurrence times of 81 days and 11 days for the intermediate-duration and short burst, respectively. These recurrence time estimates are consistent with the observed values.

For each of these examples, a decrease in accretion rate of only 40% is required to change the ignition column depth by a factor of 4 from 2 to 8×10^9 g cm^{-2}. This is because of the steep dependence of the ignition column on temperature – only a small decrease in temperature, and a small corresponding decrease in $\dot{m}$ is needed. The required decrease in accretion rate is comparable to the observed difference in persistent flux between the 2001–2002 calm period when the intermediate-duration bursts occurred and the 2003–2007 flaring period when more regular bursting resumed: as noted in Sect. 4.1, the 1-year-averaged ASM fluxes for 4U 0614+091 in 2001 and 2002 are about 30% smaller than for the years after this time interval.

It is not clear why unstable He ignition would give a nuclear energy release of only $Q_{\rm nuc} \approx 0.6$ MeV, as inferred from the burst energetics and light curve fits (see Sect. 4.2). This energy is approximately the energy released in burning He to C. For a He mass fraction Y, setting the total energy release to be $Q_{\rm nuc} = 0.6$ MeV per nucleon implies that the energy release from burning beyond C to heavy elements is $Q_{\rm heavy} \approx 0.6(1 - Y)$ MeV per nucleon. This is much less than the $\approx$1 MeV available for complete burning of C to Fe, unless the helium fraction Y is small (however, as noted above, the observations require Y to be large). At a depth of $y \sim 10^9$ g cm^{-2}, an energy deposition of

only 0.03 MeV per nucleon is sufficient to raise the temperature to above 10^9 K, at which the nuclear burning would be expected to proceed beyond C, so a significant energy release from burning beyond C would be expected. Numerical models of bursts at low accretion rates would be useful to follow the nucleosynthesis and determine the expected energy release.

Another possibility is that not all of the accreted fuel burns during the burst. For example, the burning may consume only part of the depth of the fuel layer, or may cover only part of the stellar surface. Numerical models of bursts at low accretion rates are needed to follow the nucleosynthesis and burning dynamics, and determine the expected energy release.

4.4. The superburst

In the previous section we argued that the short bursts and intermediate-duration bursts could be explained by a substantial fraction of He in the accreted material, despite the fact that the optical spectrum of 4U 0614+091 suggests that very little He is present in the accreted material. However, the superburst poses a more severe problem.

The superbursts observed in other sources at accretion rates $\dot{m} \gtrsim 0.1\,\dot{m}_{\rm Edd}$ have been explained as being due to C ignition (Strohmayer & Brown 2002; Cumming & Bildsten 2001). However, there are problems with this scenario: (1) producing enough C during H/He burning (e.g., Schatz et al. 2003; Woosley et al. 2004), (2) heating the neutron star ocean strongly enough to reach ignition temperature (e.g., Cumming et al. 2006; Keek et al. 2008), and (3) accreting rapidly enough for the C to survive to the ignition depth (Cumming & Bildsten 2001; Cumming et al. 2006).

If there is accretion of a significant amount of C from the CO white dwarf companion in 4U 0614+091, the first problem would be eased by removing the need to make the C during nuclear burning of H or He. However, if He flashes are responsible for the intermediate-duration and short bursts, the C would likely burn away during these flashes. The last two problems are more difficult to circumvent. First, the ignition temperature for C at the column depth inferred from the superburst light curve, $y \simeq 2 \times 10^{11}$ g cm^{-2}, is above 6×10^8 K. This temperature is much higher than the ignition temperatures of He flashes, i.e., about 1×10^8 K. Achieving this temperature is even more difficult when the accretion rate and therefore crust heating rate are significantly below those typical around the times of the superbursts seen in other sources. Second, we calculated models for C ignition following Cumming & Bildsten (2001) and extended their Fig. 2 to lower accretion rates, but were not able to find values of $Q_{\rm b}$ or C fraction for which the C survives to ignition depth at accretion rates of $\sim$0.01 $\dot{m}_{\rm Edd}$.

Another possibility is that ignition of a thick He layer is responsible for the observed superburst. Indeed, for the $Q_{\rm b}$ = 0.3 MeV per nucleon and $Y = 0.5$ case considered earlier, we find that reducing the local accretion rate to 1000 g cm^{-2} s^{-1}, a factor of 3 below the accretion rate that reproduces the ignition column of the intermediate-duration burst, gives He ignition at 2×10^{11} g cm^{-2}. The time scale for He burning is longer than the accumulation time (although close to it), indicating that He should survive down to the ignition depth, even for such a low accretion rate (this is not the case for the $Y = 1$, $Q_{\rm b}$ = 1 MeV per nucleon model; there we find that the He burns stably away). However, although the ignition depth can be achieved, the expected recurrence time is 9.8 yr, an order of magnitude longer than the observed time between the superburst and the previous burst, Δt = 367 days. On the other hand, this can be reconciled if an appreciable portion of the accreted He survives the preceding shorter bursts (see previous section).

Another constraint on the superburst ignition depth comes from the quenching time scale for normal bursts following the superburst. Normal bursting behaviour resumed 19 days following the superburst, the fastest time scale so far observed (see, e.g., Kuulkers 2004). Cumming & Macbeth (2004) predict that the quench time for normal bursting behaviour after a superburst is $t_{\rm quench} = 1.6 y_{12}^{3/4} (\dot{m}/\dot{m}_{\rm Edd})^{-3/4} E_{17}^{3/8}$ days (where $y = y_{12} \times 10^{12}$ g cm^{-2}). The constraint on the quench time $t_{\rm quench} < 19$ days implies for $E_{17} = 6$ and $(\dot{m}/\dot{m}_{\rm Edd}) = 0.016$ (at the time of the superburst) that $y_{12} < 0.18$. This is in good agreement with the ignition column inferred from the superburst light curve, and consistent with the normal burst observed 19 days after the superburst being the first burst to occur following the superburst. The dependencies are not very strong. For $\dot{M}/\dot{M}_{\rm Edd} = 0.0032$–$0.016$, the ignition depth is between $y_{12} < 0.04$–0.18. For $E_{17} = 1$–6 this becomes $y_{12} < 0.18$–0.44. Therefore, the quench time constraint provides another piece of evidence that the ignition depth for the superburst was lower than the depths inferred for all or most previously analysed superbursts in other sources.

5. Conclusions

We can understand several aspects of the type I X-ray bursts observed from 4U 0614+091. The column depths and energy release per gram in the bursts can be estimated by comparing the observed light curves with models, and by considering the burst energetics. Both methods are in good agreement. Helium ignition naturally explains the observed ignition depths for accretion at $\dot{m} \sim 1\%\ \dot{m}_{\rm Edd}$. Furthermore, the sensitive dependence of the He ignition depth on temperature means that small (factor of two) changes in accretion rate can lead to an order of magnitude variation among the depths, and can thereby explain the occurrence of both short bursts and intermediate-duration bursts. The ignition depth for the superburst inferred from the light curve is the lowest of the current sample of superbursts and agrees well with the constraint from the observed quenching time scale.

However, several puzzles remain. First, the amount of He required to achieve the required ignition conditions without stably burning away is significantly larger than the $\lesssim$10% limit from the optical spectra. Recently, however, formation studies using evolutionary calculations indicate that the donor in 4U 0614+091 may be a hybrid white dwarf or very evolved helium star (Nelemans et al. 2010). This suggests the donor still to be a possible supplier of a significant amount of He to the accretion disk, onto the neutron star. Further investigations have to be done, why the He does not show up then in the optical observations.

Second, understanding the superburst remains problematic. Unstable C ignition is not known to be possible at these low accretion rates: the accumulating layer is too cold, and even if heated the C burns stably. A superburst powered by a large He pile is possible, but takes several years to accumulate if the accretion rate is $\sim$1% Eddington. Such an accumulation time is much greater than the observed time of one year. Finally, the reason for the low energy per gram $Q_{\rm nuc} \lesssim 0.6$ MeV per nucleon released in the bursts is not clear.

It is important to emphasize, however, that the ignition models and light curve models used in this paper are simplified. The model light curves assume uniform and instantaneous energy deposition in the fuel layer, and do not follow the detailed nucleosynthesis. These models cannot address the early part of the

light curve, for example the interesting ripples in the early light curve of the intermediate duration burst (Fig. 10), nor whether the burning is expected to be incomplete (as we infer from the burst energetics). Incomplete burning, either across the neutron star surface or with depth in the fuel layer, may at least partly solve the above puzzles. Our ignition models rely on a simplified one-zone ignition criterion. Numerical models of accumulating and burning of He/CO mixtures at low accretion rates are needed to confirm our conclusions, for example, regarding the amount of helium needed to avoid stable burning.

It is interesting that at least in principle He can power a superburst-like event. The requirement is that the accumulating fuel layer remains cold. Recently, Cooper et al. (2009) ruled out He as a fuel for superbursts, but their argument assumed an ignition temperature of $T = 5 \times 10^8$ K that is much larger than the He ignition temperature at superburst columns. Even in the superburst sources with $\dot{m} \gtrsim 0.1\,\dot{m}_{\rm Edd}$, He-powered superbursts could occur if the accumulating layer is cold enough. One way to keep the layer cold would be to have direct URCA neutrino emission in the neutron star core, so that most of the energy release in the crust flows inwards rather than outwards. Triple alpha ignition becomes mostly sensitive to density rather than temperature when the column depth reaches $y \sim 3 \times 10^{11}$ g cm^{-2}, as the ignition becomes pycnonuclear and therefore temperature independent. This could potentially explain the narrow range of superburst ignition columns. Further work on this possibility is needed.

Acknowledgements. Partly based on observations with *INTEGRAL*, an ESA project with instruments and science data centre funded by ESA member states (especially the PI countries: Denmark, France, Germany, Italy, Switzerland, Spain), Czech Republic and Poland, and with the participation of Russia and the USA. The *RXTE*/ASM dwell average results are provided by the ASM/RXTE teams at MIT and at the RXTE SOF and GOF at NASA's GSFC. The *Swift*/BAT transient monitor results are provided by the *Swift*/BAT team. We thank Jean Swank and Lucien Kuiper for discussions regarding the bursts seen with *OSO-8* and in 2005 with *INTEGRAL*, respectively. EK thanks Andy Pollock for discussion regarding the burst recurrence times and small-number statistics. S.B. was partly supported by the Danish Space Board. A.C. acknowledges support from an NSERC Discovery Grant and the Canadian Institute for Advanced Research (CIFAR). This research has made use of the SIMBAD database, operated at CDS, Strasbourg, France.

Appendix A: Localizations of bursts

The three bursts observed by *EURECA*/WATCH had positional 3σ error circles of less than 1° radius (taking into account systematic errors and errors due to uncertainties in the spacecraft pointing). The optical (Davidsen et al. 1974; Murdin et al. 1974), infrared (Migliari et al. 2006) and radio (Migliari et al. 2010) counterparts to 4U 0614+091 were always within these error circles. The WATCH imaging results for the event which occurred on February 17 is shown in Fig. A.1 (left)[12].

At the time of the sole burst seen by the WFC, the satellite attitude solution was not optimum. However, the position for the burst is the same to within 0.1 pixel of the position determined for the persistent emission at times when the attitude solution was optimum, with an uncertainty of 2′ (99% confidence). We conclude that the origin of the burst is coincident within 2′ of the position of 4U 0614+091.

The first two bursts (in 1996 and 1998) of the six normal ASM bursts were observed by multiple SSCs, either because the burst position was in the region where the fields of view of SSC 0 and SSC 1 overlap, or because the burst was active across two sequential dwells (or both, as in the first case, yielding four independent observations). The four subsequent bursts were only detected in a single SSC for a single dwell, yielding a total of eleven observations of the six bursts (see Table A.1).

For each ASM dwell, the intensities of known sources in the field of view are derived via a fit of model slit-mask shadow patterns to counts binned by position along each anode in each detector. The residuals from a successful fit are then cross-correlated with each of the expected shadow patterns corresponding to a set of possible source directions which make up a grid covering the field of view. A peak in the resulting cross-correlation map indicates the possible presence and approximate location of a new, uncatalogued X-ray source (Levine et al. 1996; Smith et al. 1999).

To test the hypothesis that the six ASM bursts were from 4U 0614+091, we removed this source from the catalog used for the fitting procedure described. We fit the eleven observations with this truncated catalog, and we searched the residuals for evidence of a source of emission unaccounted for by the catalog. For bursts that occurred after the ASM began recording in

[12] Note that this analysis was done more than 10 years ago. Therefore, the best-fit estimates on the position of the various bursts are not available; also the regeneration of images is not possible anymore.

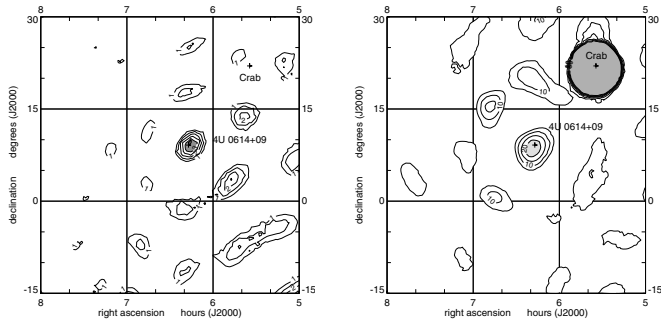

Fig. A.1. *Left*: the cross-correlation map (6−15 keV) containing the burst observed from the direction of 4U 0614+091 on February 17, 1993 by *EURECA*/WATCH. The burst was contained in a modulation pattern integrated for 56.7 s. The contours are shown in Crab units and the averaged correlation at the position of 4U 0614+091 was 3.6 Crab. Note that the integration time is too short to give a detection of the Crab. *Right*: detection of the persistent emission from 4U 0614+091 by *EURECA*/WATCH. The skymap is based on data from the period of February to April 1993 in the energy band 6−12 keV. The contours show the cross correlation in units of mCrab (only positive correlation is shown). The ring-like structure around 4U 0614+091 is an artefact caused by the WATCH RMC detection principle.

Table A.1. Observation log of ASM bursts from 4U 0614+091 (left) and 2S 0918−549 (right).

4U 0614+091			2S 0918−549		
MJD	SSC	f_X	MJD	SSC	f_X
50 200	0	0.648/0.419	50 211	0	0.418
	1	0.536/0.522	52 181	1	0.661
51 164	0, 1	0.648,0.147	52 509	0	0.208
53 476	0	0.512	52 856	0, 1	0.698, 0.230
53 959	0	0.588	53 683	1	0.671
54 101	2	0.141/0.044			
54 108	1	0.142			

Notes. Given are the day (MJD) at which the burst occurred, with which SSC it was seen (0 or 1) and the transmission factors (f_X) for the corresponding SSCs (X = 0 or 1) in the 1.5−12 keV band. For the first and fifth bursts of 4U 0614+091 we give the transmission factors for two sequential dwells, separated by a slash.

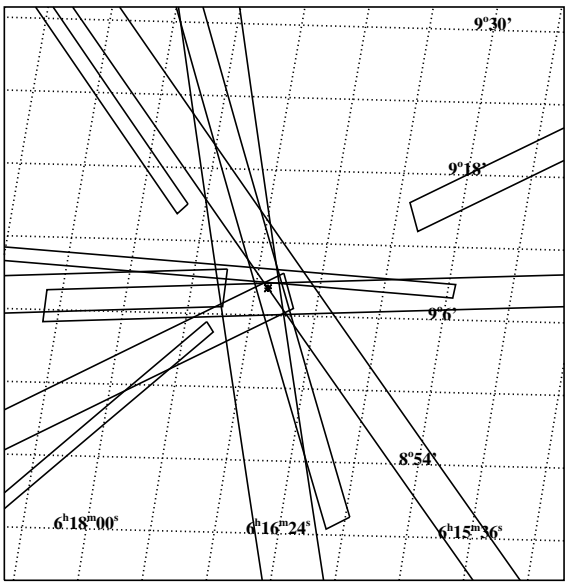

Fig. A.2. Equatorial (J2000.0) map of ten independent ASM localizations of the source of six bursts. The asterisk marks the location of the optical counterpart to 4U 0614+091 (Davidson et al. 1974; Murdin et al. 1974).

Table A.2. Positions of the bursts seen by ISGRI and BAT.

Instrument/ MJD	RA (J2000.0)	Dec	error[a]
ISGRI			
52 867	94.281°	9.152°	2.1′
53 460	94.284°	9.133°	7.0′
BAT			
54 029	94.278°	9.149°	1.5′
54 189	94.203°	9.155°	3.1′

Notes. [(a)] 90% confidence error region.

event mode, we omitted from the fit those time bins that did not show evidence of burst activity, to increase the signal to noise ratio. All eleven dwells showed evidence of a "new" source in the residuals. If 4U 0614+091 were the source of the burst in each of these dwells, the localization of this new source should be consistent with the location of 4U 0614+091.

Ten of the eleven localizations are plotted in Fig. A.2. The boxes are determined by the 95% confidence interval in each of the two dimensions recorded by the SSC, projected onto the sky. Since the two dimensions are independent, the total confidence level of the error box is about 90%. These uncertainties are statistical only. The location of the optical counterpart of 4U 0614+091 is indicated by an asterisk. This location cannot be excluded by any of the error boxes, including an eleventh error box that lies outside the limits of this plot.

For ten of the thirteen FREGATE bursts a precise localization was possible using the WXM and/or SXC, and they are consistent with coming from 4U 0614+091 (see Sect. 2.1.5). For the other three bursts we can only suppose they are coming from 4U 0614+091, since the source was the only persistent burster in the FREGATE field of view.

The reconstructed 15–30 keV images of the field of view around 4U 0614+091 during the bursts seen by ISGRI are shown in Fig. A.3. The only two detected sources in the 2003 (24 s) and 2005 (15 s) time frames are indeed 4U 0614+091, as well

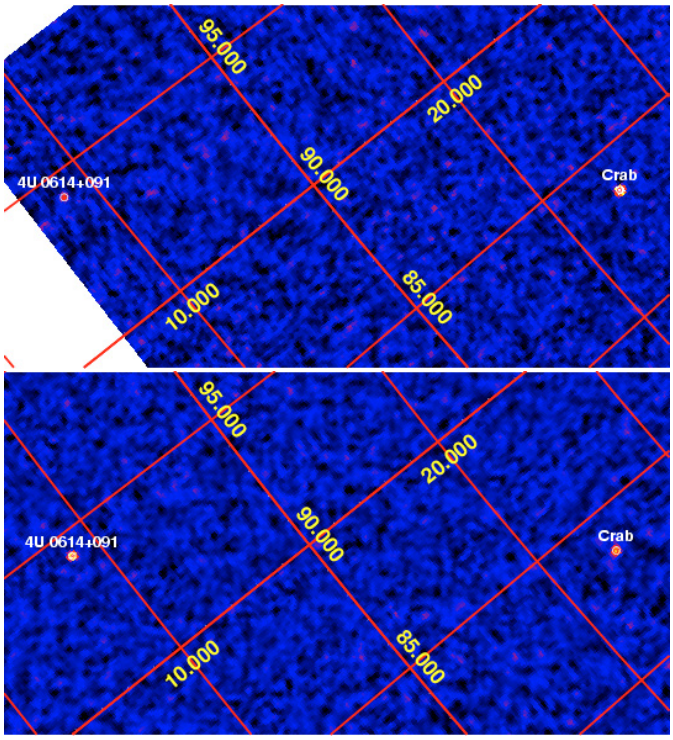

Fig. A.3. IBIS/ISGRI (15–30 keV) significance images during the bursts detected on 2003 August 16 (*top*) and 2005 March 31 (*bottom*). Shown is the equatorial J2000.0 grid with 5° spacing. 4U 0614+091 and Crab are the only sources detected in the time frames (UT 21:30:18−21:30:43 and UT 07:12:18−07:12:34, respectively). The detection significances of 4U 0614+091 (and Crab) in the 2003 and 2005 time frames are 4.7 (18.3) and 12.7 (6.9), respectively.

as the persistently bright Crab source. The data from the two BAT bursts were subjected to the post "γ-ray burst" processing script, which led to refined positions for these bursts. The derived ISGRI and BAT bursts coordinates are given in Table A.2. They are also consistent with the optical, IR and radio counterparts to 4U 0614+091.

We conclude that the 27 bursts seen by *EURECA*/WATCH, WFC, ASM, FREGATE, ISGRI and BAT indeed originated from 4U 0614+091.

References

Atteia, J.-L., Boer, M., Cotin, F., et al. 2003, in Gamma-Ray Burst and Afterglow Astronomy 2001, ed. G. Ricker, & R. Vanderspek (New York: AIP), AIP Conf. Proc., 662, 17
Barraud, C. 2002, presentation given at the AMS Workshop on Sources and GRBs, 6/12/2002, Montpellier, France
Barret, D., & Grindlay, J. E. 1995, ApJ, 440, 841
Barthelmy, S. D., Barbier, L. M., Cummings, J. R., et al. 2005, SSRv, 120, 143
Belian, R. D., Conner, J. P., & Evans, W. D. 1976, ApJ, 206, L135
Bildsten, L., Salpeter, E., & Wasserman, I. 1992, ApJ, 384, 143
Boella, G., Butler, R. C., Perola, G. C., et al. 1997, A&A, 122, 299
Bradt, H. V., Rothschild, R. E., & Swank, J. H. 1993, A&AS, 97, 355
Brandt, S. 1994, Ph.D. Thesis, DSRI, Denmark
Brandt, S., & Lund, N. 1995, Adv. Space Res., 16(8), 37
Brandt, S., Castro-Tirado, A. J., Lund, N., et al. 1992, A&A, 262, L15
Brandt, S., Lund, N., & Rao, A. R. 1990, Adv. Space Res., 10(2), 239
Brandt, S., Lund, N., & Castro-Tirado, A. J. 1993a, IAU Circ., 5710
Brandt, S., Lund, N., & Castro-Tirado, A. J. 1993b, IAU Circ., 5717
Brown, E. F. 2000, ApJ, 531, 988
Brown, E. F., & Bildsten, L. 1998, ApJ, 496, 915
Buccheri, R., Bennett, K., Bignami, G. F., et al. 1983, A&A, 128, 245
Chelovekov, I. V., Grebenev, S. A., & Sunyaev, R. A. 2007, Proceedings of the 6th INTEGRAL Workshop, The Obscured Universe, ESA SP-622, 445

Cocchi, M., Bazzano, A., Natalucci, L., et al. 2000, A&A, 357, 527
Cooper, R. L., Steiner, A. W., & Brown, E. F. 2009, ApJ, 702, 660
Cornelisse, R., Heise, J., Kuulkers, E., Verbunt, F., & in 't Zand, J. J. M. 2000, A&A, 357, L21
Cornelisse, R., Kuulkers, E., in 't Zand, J. J. M., Verbunt, F., & Heise, J. 2002a, A&A, 382, 174
Cornelisse, R., Verbunt, F., in 't Zand, J. J. M., et al. 2002b, A&A, 392, 885
Cornelisse, R., in 't Zand, J. J. M., Verbunt, F., et al. 2003, A&A, 405, 1033
Courvoisier, T. J.-L., Walter, R., Beckmann, V., et al. 2003, A&A, 411, L53
Cumming, A. 2004, Nuc. Phys. B Proc. Suppl., 132, 435
Cumming, A., & Bildsten, L. 2001, ApJ, 559, L127
Cumming, A., & Macbeth, J. 2004, ApJ, 603, L37
Cumming, A., Macbeth, J., in 't Zand, J. J. M., & Page, D. 2006, ApJ, 646, 429
Davidsen, A., Malina, R., Smith, H., et al. 1974, ApJ, 193, L25
Ebisawa, K., Bourban, G., Bodaghee, A., Mowlavi, N., & Courvoisier, T. J.-L. 2003, A&A, 411, L59
Falanga, M., Chenevez, J., Cumming, A., et al. 2008, A&A, 484, 43
Falanga, M., Cumming, A., Bozzo, E., & Chenevez, J. 2009, A&A, 496, 333
Fiocchi, M., Bazzano, A., Ubertini, P., et al. 2008, A&A, 492, 557
Ford, E., Kaaret, P., Tavani, M., et al. 1996, ApJ, 469, L37
Ford, E. C., Kaaret, P., Chen, K., et al. 1997, ApJ, 486, L47
Ford, E. C., van der Klis, M., Méndez, M., et al. 2000, ApJ, 537, 368
Galloway, D. K., Muno, M. P., Hartman, J. M., et al. 2008, ApJS, 179, 360
Gehrels, N., Chincarini, G., Giommi, P., et al. 2004, ApJ, 611, 1005
Giacconi, R., Murray, S., Gursky, H., et al. 1972, ApJ, 178, 281
Goldwurm, A., David, P., Foschini, L., et al. 2003, A&A, 411, L223
Grindlay, J., Gursky, H., Schnopper, H., et al. 1975, ApJ, 205, L127
Hansen, C. J., & van Horn, H. M. 1975, ApJ, 195, 735
Harmon, B. A., Wilson, C. A., Fishman, G. J., et al. 2004, ApJS, 154, 585
Hasinger, G., & van der Klis, M. 1989, A&A, 225, 79
Hoffman, J. A., Marshall, H. L., & Lewin, W. H. G. 1978, Nature, 271, 630
in Zand, J. J. M. 1992, Ph.D. Thesis, Utrecht University
in 't Zand, J. J. M., Cumming, A., van der Sluys, M. V., Verbunt, F., & Pols, O. R. 2005, A&A, 441, 675
in 't Zand, J. J. M., Bassa, C. G., Jonker, P. G., et al. 2008, A&A, 485, 183
in 't Zand, J. J. M., Jonker, P. G., & Markwardt, C. B. 2007, A&A, 465, 953
in 't Zand, J. J. M., Keek, L., Cumming, A., et al. 2009, A&A, 497, 469
Jager, R., Mels, W. A., Brinkman, A. C., et al. 1997, A&A, 125, 557
Jahoda, K., Markwardt, C. B., Radeva, Y., et al. 2006, ApJS, 163, 401
Jonker, P. G., & Nelemans, G. 2004, MNRAS, 354, 355
Juett, A. M., & Chakrabarty, D. 2003, ApJ, 599, 498
Juett, A. M., Psaltis, D., & Chakrabarty, D. 2001, ApJ, 560, L59
Keek, L., & in 't Zand, J. J. M. 2009, in proceedings of the 7th INTEGRAL Workshop, An INTEGRAL View of Compact Objects, PoS(Integral08)032
Keek, L., in 't Zand, J. J. M., Kuulkers, E., et al. 2008, A&A, 479, 177
Krimm, H., Barbier, L., Barthelmy, S. D., et al. 2006, ATel, #904
Kuulkers, E. 2002, A&A, 383, L5
Kuulkers, E. 2004, Nuc. Phys. B Proc. Suppl., 132, 466
Kuulkers, E. 2005, ATel, #483
Kuulkers, E., den Hartog, P. R., in 't Zand, J. J. M., et al. 2003, A&A, 399, 663
Kuulkers, E., in 't Zand, J. J. M., van Kerkwijk, M. H., et al. 2002a, A&A, 382, 503
Kuulkers, E., Homan, J., van der Klis, M., Lewin, W. H. G., & Méndez, M. 2002b, A&A, 382, 947
Kuulkers, E., Shaw, S. E., Paizis, A., et al. 2007, A&A, 466, 595
Kuulkers, E., van der Klis, M., Oosterbroek, T., et al. 1994, A&A, 289, 795
Lamb, D. Q., & Lamb, F. K. 1978, ApJ, 220, 291
Lebrun, F., Leray, J. P., Lavocat, P., et al. 2003, A&A, 411, L141
Levine, A. M., Bradt, H., Cui, W., et al. 1996, ApJ, 469, L33
Lewin, W. H. G. 1976, IAU Circ., 2914
Lewin, W. H. G., Vacca, W. D., & Basinska, E. M. 1984, ApJ, 277, L57
Lewin, W. H. G., van Paradijs, J., & Taam, R. E. 1993, SSRv, 62, 223
Linares, M., Watts, A. L., Wijnands, R., et al. 2009, MNRAS, 392, L11
Lund, N. 1985, in X-Ray Instrumentation in Astronomy, ed. J. L. Culhane, Porc. SPIE, 597, 95
Lund, N., Brandt, S., Budtz-Jørgensen, C., et al. 2003, 411, L231
Maraschi, L., & Cavaliere, A. 1977, in Highlights in Astronomy, ed. E. A. Müller, 4, 127
Markert, T. H., Laird, F. N., Clark, G. W., et al. 1979, ApJS, 39, 573
Mason, K. O., Charles, P. A., White, N. E., et al. 1976, MNRAS, 177, 513
Méndez, M., Cottam, J., & Paerels, F. 2002 [arXiv:astro-ph/0207277]
Mereghetti, S., Götz, D., Borkowski, J., Walter, R., & Pedersen, H. 2003, A&A, 411, L291
Migliari, S., & Fender, R. 2006, MNRAS, 366, 79
Migliari, S., Tomsick, J. A., Maccarone, T. J., et al. 2006, ApJ, 643, L41
Migliari, S., Tomsick, J. A., Miller-Jones, J. C. A., et al. 2010, ApJ, 710, 117
Molkov, S. V., Grebenev, S. A., & Lutovinov, A. A. 2000, 357, L41
Murdin, P., Penston, M. J., Penston, M. V., et al. 1974, MNRAS, 169, 25
Nelemans, G., Jonker, P. G., Marsh, T. R., & van der Klis, M. 2003, MNRAS, 348, L7
Nelemans, G., Jonker, P. G., & Steeghs, D. 2006, MNRAS, 370, 255
Nelemans, G., Yungelson, L. R., van der Sluys, M. V., & Tout, C. A. 2010, MNRAS, 401, 1347
Parsignault, D. R., & Grindlay, J. E. 1978, ApJ, 225, 970
Piraino, S., Santangelo, A., Ford, E. C., & Kaaret, P. 1999, A&A, 349, L77
Ricker, G. R., Atteia, J.-L., Crew, G. B., et al. 2003, in Gamma-Ray Burst and Afterglow Astronomy 2001: A Workshop Celebrating the First Year of the HETE Mission, ed. G. R. Ricker, & R. K. Vanderspek, AIP Conf. Ser., 662, 3
Rothschild, R. E., Blanco, P. R., Gruber, D. E., et al. 1998, ApJ, 496, 538
Schatz, H., Bildsten, L., & Cumming, A. 2003, ApJ, 583, L87
Shahbaz, T., Watson, C. A., Zurita, C., Villaver, E., & Hernandez-Peralta, H. 2008, PASP, 120, 848
Shirasaki, Y., Kawai, N., Yoshida, A., et al. 2003, PASJ, 55, 1033
Smith, D. A., Levine, A. M., Bradt, H. V., et al. 1999, ApJ, 526, 683
Strohmayer, T., & Bildsten, L. 2006, in Compact stellar X-ray sources, ed. W. H. G. Lewin, & M. van der Klis, Cambridge Astrophys. Ser., 39, 113
Strohmayer, T. E., & Brown, E. F. 2002, ApJ, 566, 1045
Strohmayer, T. E., & Markwardt, C. B. 2002, ApJ, 577, 337
Strohmayer, T. E., Markwardt, C. B., & Kuulkers, E. 2008, ApJ, 672, L37
Suzuki, M., Sakamoto, T., Takahashi, D., et al. 2004, in Third Rome Workshop on Gamma-Ray Bursts in the Afterglow Era, ed. M. Feroci, F. Frontera, N. Masetti, & L. Piro, ASP Conf. Ser., 312, 138
Swank, J. H., Becker, R. H., Boldt, E. A., Holt, S. S., & Serlemitsos, P. J. 1978, MNRAS, 182, 349
Tawara, Y., Kii, T., Hayakawa, S., et al. 1984, ApJ, 276, L41
Ubertini, P., Lebrun, F., Di Cocco, G., et al. 2003, A&A, 411, L131
van der Klis, M. 1995, in The Lives of the Neutron Stars, ed. M. A. Alpar, Ü. Kızıloğlu, & J. van Paradijs (Kluwer Academic Publishers), NATO ASI Ser. C, 450, 301
van Paradijs, J., & Lewin, W. H. G. 1986, A&A, 157, L10
van Straaten, S., Ford, E. C., van der Klis, M., Méndez, M., & Kaaret, P. 2000, ApJ, 540, 1049
van Straaten, S., van der Klis, M., & Méndez, M. 2003, ApJ, 596, 1155
Verner, D. A., Ferland, G. J., Korista, K. T., & Yakovlev, D. G. 1996, ApJ, 465, 487
Villasenor, J. N., Dill, R., Doty, J. P., et al. 2003, in Gamma-Ray Burst and Afterglow Astronomy 2001: A Workshop Celebrating the First Year of the HETE Mission, ed. G. R. Ricker, & R. K. Vanderspek, AIP Conf. Ser., 662, 33
Warwick, R. S., Marshall, N., Fraser, G. W., et al. 1981, MNRAS, 197, 865
Werner, K., Nagel, T., Rauch, T., Hammer, N. J., & Dreizler, S. 2006, A&A, 450, 725
Westergaard, N. J., Kretschmar, P., Oxborrow, C. A., et al. 2003, A&A, 411, L257
Wijnands, R. 2001, ApJ, 554, L59
Wilms, J., Allen, A., & McGray, R. 2000, ApJ, 542, 914
Winkler, C., Courvoisier, T. J.-L., Di Cocco, G., et al. 2003, A&A, 411, L1
Woosley, S. E., & Taam, R. E. 1976, Nature, 263, 101
Woosley, S. E., Heger, A., Cumming, A., et al. 2004, ApJS, 151, 75